TMEM8C-mediated fusion is regionalized and regulated by NOTCH signalling during foetal myogenesis

Joana Esteves de Lima, Cédrine Blavet, Marie-Ange Bonnin, Estelle Hirsinger, Emmanuelle Havis, Frédéric Relaix, Delphine Duprez

TMEM8C-mediated fusion is regionalized and regulated by NOTCH signalling during foetal myogenesis

Joana Esteves de Lima[1,2,*], Cédrine Blavet[1], Marie-Ange Bonnin[1], Estelle Hirsinger[1], Emmanuelle Havis[1], Frédéric Relaix[2] and Delphine Duprez[1,*]

[1] Sorbonne Université, Institut Biologie Paris Seine, CNRS UMR7622, Developmental Biology Laboratory, Inserm U1156, F-75005 Paris, France.

[2] Univ Paris Est Creteil, INSERM, EnvA, EFS, AP-HP, IMRB, F-94010 Creteil, France

* Corresponding authors

E-mail: delphine.duprez@sorbonne-universite.fr

E-mail: joana.esteves-de-lima@inserm.fr

Key words: TMEM8C, MYOG, NOTCH, HEYL, myoblast fusion, foetal myogenesis

Summary statement

Myomaker+ fusion-competent myoblasts are preferentially localized to the central part of the foetal muscle, suggesting a central regionalization of myoblast fusion. NOTCH signalling transcriptionally regulates the myomaker-dependent fusion gene.

Abstract

The location and regulation of fusion events within skeletal muscles during development remain unknown. Using the fusion marker myomaker (*Mymk*), named *TMEM8C* in chicken, as a readout of fusion, we identified a co-segregation of *TMEM8C*-positive cells and *MYOG*-positive cells in single-cell RNA-sequencing datasets of limbs from chicken embryos. We found that *TMEM8C* transcripts, *MYOG* transcripts and the fusion-competent MYOG-positive cells were preferentially regionalized in central regions of foetal muscles. We also identified a similar regionalization for the NOTCH ligand *JAGGED2* along with an absence of NOTCH activity in *TMEM8C*+ fusion-competent myocytes. NOTCH function in myoblast fusion had not been addressed so far. We analysed the consequences of NOTCH inhibition for *TMEM8C* expression and myoblast fusion during foetal myogenesis in chicken embryos.

NOTCH inhibition increased myoblast fusion and *TMEM8C* expression and released the HEYL transcriptional repressor from the *TMEM8C* regulatory regions. These results identify a regionalization of *TMEM8C*-dependent fusion and a molecular mechanism underlying the fusion-inhibiting effect of NOTCH in foetal myogenesis. The modulation of NOTCH activity in the fusion zone could regulate the flux of fusion events.

Introduction

Skeletal muscle development, homeostasis and regeneration rely on muscle progenitors and stem cells that undergo a multistep process to form multinucleated cells named myofibres. The myofibres are formed by myoblast fusion and constitute the main structural unit of skeletal muscles. The fusion of myoblasts has been poorly studied and remains challenging to study in vivo because it is difficult to dissociate the differentiation and fusion processes during myogenesis. Moreover, the location of fusion events within the developing muscles remains unknown.

The transcriptional control of the skeletal muscle programme is dependent on four bHLH transcription factors, MYF5, MRF4, MYOD and MYOG, named the Myogenic Regulatory Factors (MRFs) (Buckingham and Rigby, 2014). MRFs have the ability to trigger the muscle programme including the successive steps of specification, commitment, differentiation and fusion from muscle progenitors (Buckingham and Rigby, 2014; Comai and Tajbakhsh, 2014; Esteves de Lima and Relaix, 2021), but also from non-muscle cells in vitro and in vivo (Delfini and Duprez, 2004; Weintraub et al., 1991). Multinucleated myofibre formation is a multistep process involving cell cycle withdrawal of already committed myoblasts, cell elongation, cell-cell contact and fusion (Biressi et al., 2007; Comai and Tajbakhsh, 2014). The three main steps that underlie myoblast fusion are: (1) cell recognition and adhesion; (2) enhancement of cell proximity via F-actin-propelled membrane protrusions from one fusion partner cell and myosin II-dependent cortical tension in the other fusion partner cell; (3) destabilization of the two apposed plasma membrane lipid bilayers and formation of a fusion pore (Hernández and Podbilewicz, 2017; Kim et al., 2015). Numerous transmembrane proteins and molecules of the intracellular actin machinery are involved in myoblast fusion in vertebrates. However, these proteins are not specific to myoblast fusion and are recruited for any cell-cell fusion processes such as sperm-egg fusion in fertilisation, cytotrophoblast fusion in placentation and axonal fusion during neuronal repair (Hernández and Podbilewicz, 2017). Recently, a muscle-specific gene, myomaker (named *TMEM8C* in chicken, *Mymk* in mice and *MYMK* in humans) has been identified as being essential for myoblast fusion in mice,

chicken and zebrafish during development and muscle regeneration (Landemaine et al., 2014; Luo et al., 2015; Millay et al., 2013, 2014, 2016). Myomaker is a transmembrane protein of 221 amino acids with seven membrane-spanning regions. Autosomal recessive mutations in the *MYMK* gene, which reduce but do not eliminate *MYMK* function, cause a congenital myopathy, the Carey-Fineman-Ziter syndrome, in humans (Di Gioia et al., 2017). Myomaker is sufficient to trigger fibroblast-myoblast fusion but not fibroblast-fibroblast fusion (Millay et al., 2014). However, when combined with the micropeptide myomixer (also named myomerger or minion), myomaker triggers fibroblast-fibroblast fusion (Bi et al., 2017; Quinn et al., 2017; Zhang et al., 2017). By itself, myomixer does not possess 10T1/2 fibroblast-C2C12 myoblast fusion activity (Bi et al., 2017). Two MRFs, MYOD and MYOG, have been shown to positively regulate the transcription of *myomaker* genes in mouse, zebrafish and chicken via E-boxes located in the *myomaker* promoter regions (Ganassi et al., 2018; Luo et al., 2015; Millay et al., 2014). The direct transcriptional regulation of the *myomaker* gene by MRFs couples the differentiation and fusion processes making it complex to study them independently.

NOTCH signalling is recognized to being involved in skeletal muscle differentiation during development. NOTCH inhibition promotes muscle differentiation in both in vivo and in vitro systems (Kitzmann et al., 2006; Kopan et al., 1994; Schuster-Gossler et al., 2007; Vasyutina et al., 2007). Conversely, NOTCH is a potent inhibitor of muscle differentiation in chicken and mouse models during embryonic and foetal myogenesis (Bonnet et al., 2010; Delfini and Duprez, 2004; Esteves de Lima et al., 2016; Hirsinger et al., 2001; Mourikis et al., 2012a; Vasyutina et al., 2007; Zalc et al., 2014). Active NOTCH also inhibits muscle differentiation in C2C12 cells (Kopan et al., 1994; Kuroda et al., 1999). NOTCH displays additional functions in postnatal myogenesis, since NOTCH is required to maintain the quiescence and to regulate the migratory behaviour of satellite cells (Baghdadi et al., 2018; Bjornson et al., 2012; Conboy and Rando, 2002; Conboy et al., 2003, 2005; Mourikis et al., 2012b). The canonical NOTCH pathway mediates cell-to-cell communication involving a transmembrane NOTCH receptor and a transmembrane NOTCH ligand. Upon ligand activation, the NOTCH receptor undergoes a proteolytic cleavage to produce the NOTCH intracellular domain (NICD) that translocates to the nucleus and interacts with RBPJ to regulate gene transcription (Andersson et al., 2011; Kopan et al., 1994; Lubman et al., 2007). NICD immediate transcriptome and ChIP-sequencing analyses identified key genes activated downstream of NOTCH, which include the bHLH transcriptional repressors, *Hes* (Hairy and enhancer of split) and *Hey* (Hairy/enhancer-of-split related with YRPW motif) genes

(Andersson et al., 2011). During mouse foetal myogenesis, *Heyl* is the main transcriptional response to NICD (Mourikis et al., 2012a). HES and HEY proteins repress the transcription of muscle differentiation genes to maintain muscle cells in a progenitor state in mice (Bröhl et al., 2012; Fukada et al., 2011; Lahmann et al., 2019; Mourikis et al., 2012a; Noguchi et al., 2019; Zalc et al., 2014). Because NOTCH is involved in muscle differentiation, NOTCH function in myoblast fusion is difficult to address. No link has been established between components of the NOTCH intracellular pathway and the fusion gene *myomaker*.

The identification of myomaker as a transmembrane protein required for myoblast fusion (Millay et al., 2013) stimulated the research on muscle fusion. However, the signalling pathways that regulate *myomaker* expression are not fully identified. Moreover, the location of fusion events within muscles remains to be understood in vivo. Here, we identify a regionalized location within foetal muscles for the key molecular actors involved in myoblast fusion and the NOTCH ligand *JAGGED2* (*JAG2*). We also identified NOTCH as a regulator of *TMEM8C* expression and of the fusion process during foetal myogenesis using in vitro and in vivo chicken systems.

Materials and methods

Chicken embryos

Fertilized chicken (*Gallus gallus*) eggs from commercial sources (White Leghorn strain, HAAS, Strasbourg, France and JA 57 strain, Morizeau, Dangers, France) were incubated at 38.5°C in a humidified incubator until appropriate stages. Embryos were staged according to the number of days in ovo (E). All experiments on chicken embryos were performed before E14 and consequently are not submitted to a licensing committee, in accordance to the European guidelines and regulations.

Single-cell RNA-sequencing analysis from whole limb cells

The scRNAseq protocol and sample collection is described in Esteves de Lima et al., 2021. The sequencing data has been deposited in the NCBI Gene Expression Omnibus database (https://www.ncbi.nlm.nih.gov/geo/) with the accession number GSE166981. Briefly, scRNAseq datasets were generated from whole forelimbs from 3 different E6 embryos and 3 different E10 embryos using the 10X Chromium Chip (10X Genomics) followed by sequencing with a HighOutput flowcel using an Illumina Nextseq 500 and by sequence analysis with Cell Ranger Single Cell Software Suite 3.0.2 (10X Genomics). Only mononucleated muscle cells are included in the datasets, since the plurinucleated myotubes

are excluded by the single-cell isolation protocol. The Seurat package (v3.0) (Stuart et al., 2019) under R (v3.6.1) (R Core Team, 2019) was used to perform downstream clustering analysis on scRNAseq data (Macosko et al., 2015). We then extracted the clusters identified as muscle clusters by the differential expression of classical myogenic markers (*PAX7, MYOD, MYOG, MYHC*) and performed the rest of the analysis on these muscle clusters only. Gene expression is defined by "gene Log-normalized count > 0". The scRNAseq datasets were analysed using Seurat tools such as Feature plots and Violin plots. The R package ggplot2 v3.3.3 (Wickham, 2016) was used to generate custom feature plots highlighting gene co-expression. Population intersection plots were generated with the R package UpSetR v1.4.0 (Conway et al., 2017).

Chemical inhibitor administration

Decamethonium bromide (DMB) (Sigma) solution and control Hank's solution were prepared as previously described (Esteves de Lima et al., 2016). 100 µl of DMB or control solutions were administered in chicken embryos at E7.5 and E8.5. Embryos were collected at E9.5.

Grafts of DELTA1/RCAS-expressing cells

Chicken embryonic fibroblasts (CEFs) obtained from E10 chicken embryos were transfected with DELTA1/RCAS using the Calcium Phosphate Transfection Kit (Invitrogen). Cell pellets of approximately 50–100 µm in diameter were grafted into limb buds of E4.5 embryos as previously described (Bonnet et al., 2010; Delfini et al., 2000). DELTA1/RCAS-grafted embryos were harvested at E6.5 or E9.5. The embryos collected at E9.5 were treated with DMB or control solutions at E7.5 and E8.5.

Somite electroporation

Forelimb somite electroporation was performed as previously described (Wang et al., 2011). The DNA solution was composed of the pT2AL-MLC-Tomato-DELTA1/DN or the pT2AL-MLC-Tomato (control) vectors and a transient transposase-containing vector CMV/βactin-T2TP (Bourgeois et al., 2015; Esteves de Lima et al., 2016). This vector set allows the stable integration of the MLC-Tomato-DELTA1-DN or the MLC-Tomato cassettes into the chick genome. The concentration of each vector was 2 µg/µL and of 1/3 for the CMV/βactin-T2TP. DNA was prepared in solution containing carboxymethyl cellulose 0,17% (Sigma), fast green 1% (Sigma), $MgCl_2$ 1 mM (VWR Chemicals) and PBS 1X in water.

Myoblast cultures

Primary myoblasts were obtained from hindlimbs of E10 chicken embryos and cultured in proliferating high-serum-containing medium (10%) or in differentiation low-serum-containing medium (2%), as previously described (Havis et al., 2012). For NOTCH gain-of-function experiments, myoblasts were transfected with DELTA1/RCAS plasmid or Empty/RCAS (control). We performed NOTCH loss-of-function experiments in myoblasts using the γ-secretase inhibitor DAPT (Sigma). For NOTCH loss-of-function experiments, myoblasts were treated with DAPT (Sigma) at a concentration of 5 µM for 24 h in low and high serum conditions (proliferation and differentiation assays) versus DMSO (Fluka) (controls). For the fusion assay MYOG+ myoblasts plated at a high density in low serum conditions (Girardi et al., 2021; Latroche et al., 2017) were treated with 5 µM DAPT (Sigma) at 0 h and 24 h of culture and collected at 48 h.

Immunohistochemistry

Forelimbs of control and manipulated (DMB, DELTA1/RCAS) chicken embryos were fixed in 4% paraformaldehyde (Sigma) overnight at 4°C and then processed in gelatin/sucrose (Sigma) for 12 µm cryostat sections as previously described (Esteves de Lima et al., 2014). The monoclonal antibodies, PAX7 and MF20 developed by D.A. Fischman and A. Kawakami, respectively, were obtained from the Developmental Studies Hybridoma Bank developed under the auspices of the NICHD and maintained by the University of Iowa, Department of Biology Iowa City, IA 52242. The Collagen XII and MYOG antibodies were kindly provided by Manuel Koch (Germany) (Koch et al., 1992) and Christophe Marcelle (France) (Manceau et al., 2008), respectively. The MYOD (BD Biosciences) and pSMAD1/5/9 (Cell Signalling) antibodies were obtained from commercial sources. Secondary antibodies were conjugated with Alexa-488, Alexa-555 or Alexa-647 (Invitrogen). Nuclei were visualised with DAPI (Sigma) staining. Antibody detailed information is stated in Table S1.

In situ hybridization

Chicken forelimbs of control and manipulated (DMB, DELTA1/RCAS, DELTA1-DN) embryos were fixed in 4% paraformaldehyde (Sigma) overnight at 4°C and processed for in situ hybridization on wax tissue or cryostat sections, as previously described (Esteves de Lima et al., 2016). The digoxigenin-labelled mRNA probes were prepared as previously described: MYOD, JAG2 and DLL1 (Delfini et al., 2000), FGF4 and SCX (Edom-Vovard et

al., 2001), MYOG (Bonnet et al., 2010). The TMEM8C probe was obtained by PCR from E9.5 limb tissues using the following primers: Fw: 5'-ACCCTCAGCACTTTGGTCTTT-3' and Rv: 5'-ACAGGGCACACCCCATACA-3', cloned into the pCRII-TOPO vector (Invitrogen), linearized with NotI (Biolabs) and synthetized with SP6 (Promega). Fluorescent in situ hybridization was performed according to (Wilmerding et al., 2021).

RNA extraction and Real-Time quantitative PCR (RT-qPCR)

Total RNAs were extracted from control limbs, experimental limbs or primary foetal myoblast cultures. 500 ng to 1 µg of RNA was reverse-transcribed using the High-Capacity Retrotranscription kit (Applied Biosystems). RT-qPCR was performed using SYBR Green PCR Master Mix (Applied Biosystems). Primer sequences used for RT-qPCR are listed in Table S2. The relative mRNA levels were calculated using the 2^-ΔΔCt method (Livak and Schmittgen, 2001; Schmittgen and Livak, 2008). The ΔCts were obtained from Ct normalized with *GAPDH* and *RPS17* levels in each sample. Each RNA sample was analysed in duplicate.

Chromatin immunoprecipitation assay

In vitro ChIP assay was performed as previously described (Harada et al., 2018). In vivo ChIP assay was performed as previously described (Havis et al., 2006). Limbs from E9.5 chicken embryos were homogenized using a mechanical disruption device (Lysing Matrix A, Fast Prep MP1, 2x40 s at 6 m/s, Machine MP Bio). 5 µg of the HEYL antibody, kindly provided by So-Ichiro Fukada (Osaka University, Japan) (Fukada et al., 2007), were used to immunoprecipitate 10 µg of sonicated chromatin. ChIP products were analysed by RT-qPCR to amplify the target regions. The primer list is shown in Table S2.

Image capture

After immunohistochemistry or in situ hybridization experiments, images were obtained using a Zeiss apotome epifluorescence microscope, a Leica DMI600B fluorescence microscope or a Leica SP5 confocal system.

Image analyses and quantification

For the distribution of MYOG+ and PAX7+ cells in the middle versus the tips of muscle, the MYOG/DAPI or PAX7/DAPI percentage is the number of MYOG+ or PAX7+ nuclei in each region divided by the total number of DAPI+ nuclei in that region. The number of PAX7+ and MYOG+ cells in control and DAPT foetal myoblast cultures was normalised to the

number of total DAPI+ nuclei. The fusion index is the number of nuclei within myotubes (MF20+) (2 nuclei at the minimum) divided by the total number of DAPI+ nuclei in the field. For the distribution of the number of myonuclei per fibre, the fibre percentage is the number of fibres with a given number of myonuclei divided by the total number of fibres. All the described quantifications were performed using the Cell counter plug-in of the free softwares Image J or Fiji (Schneider et al., 2012).

Statistical analyses

Data was analysed using the non-parametric two-tailed test, Mann-Whitney test using the Graphpad Prism V6 software, except for the ChIP-RT-qPCR samples that were analysed with the two-tailed paired *t*-test. Results are shown as means±standard deviation (s.d.). The *p*-values are indicated either with the number on the graphs or with asterisks. Asterisks indicate the following *p*-values: *p<0.05, **p<0.01, ***p<0.001 and ****p<0.0001. No data were excluded. No randomization was allocated between the samples since we compared control and treated animals / samples. Blinding was used to perform image acquirement and quantification.

Results

scRNAseq analysis shows that *TMEM8C*+ fusion competent cells co-express *MYOD* and *MYOG* in chicken limb foetal muscles

Given the requirement and sufficiency of *TMEM8C* (*Myomaker*) for myoblast fusion (Millay et al., 2013), we used *TMEM8C* gene as a readout for muscle fusion. We first analysed the distribution of *TMEM8C*+ fusion-competent cells in single-cell RNA-sequencing (scRNAseq) datasets of chicken whole limb cells at the E6 and E10 foetal stages. At E6, the transition time point between the end of embryonic myogenesis and the initiation of foetal myogenesis (Duprez, 2002), limb muscles are not yet individualized and spatially organised, while at E10 the final limb muscle pattern is set. We performed a Seurat-based clustering analysis, described elsewhere (Esteves de Lima et al., 2021), leading to the identification of all the limb cell clusters. As the focus of our study is muscle fusion, we will only consider the muscle clusters (Fig. S1A,B) for this analysis. At E6, myogenic cells are segregated in two muscle clusters, the PAX7 (progenitor) and the MYOD/MYOG (myogenic) clusters (Fig. 1A), as evidenced by the differential expression of the *PAX7*, *MYOD* and *MYOG* genes in these clusters (Fig. S1C). At E10, the myogenic cell segregation can be further refined in four clusters, the PAX7, MYOD, MYOD/MYOG and Myosin clusters (Fig. 1D and S1D), illustrating the cell progression through the canonical myogenic maturation steps. At both E6

and E10 stages, *TMEM8C*+ cells are mainly located in the *MYOD/MYOG* cluster, rather than in PAX7 (progenitor) or Myosin clusters (Fig. 1B,E for feature plots and 1C,F for VlnPlots). We further analysed the co-expression of *TMEM8C* and myogenic markers (*PAX7*, *MYOD*, *MYOG*) at the single cell level (Fig. 1G,H,I). At E6 and E10, fusion-competent *TMEM8C*+ myogenic cells represent 56.5% and 33.2% of the *MYOG*+ cells, respectively, which is the highest proportion compared to that for the *PAX7*+ (4.8 % at E6 and 0.7 % at E10) and *MYOD*+ (17.6 % at E6 and 12.5 % at E10) populations (Fig. 1I, upper panel). Conversely, the repartition of *TMEM8C*+ cells across the *PAX7*+, *MYOD*+ and *MYOG*+ populations shows that the majority of the *TMEM8C*+ cells are not in a *PAX7*+ progenitor state but rather in *MYOD*+ and *MYOG*+ advanced states of myogenic differentiation. For example, *MYOG*+ cells represent 72.2% and 60.5% of TMEM8C+ cells at E6 and E10, respectively (Fig. 1I, lower panel). The frequency of the combinations that include *MYOD* and/or *MYOG* amounts to 75% and 84% of the *TMEM8C*+ cells at E6 and E10, respectively. These frequencies are higher than those of corresponding combinations within the total myogenic (*PAX7*+, *MYOD*+ or *MYOG*+) population (39.6% at E6 and 54.8% at E10) (Fig. S1E,F,G, right panels), suggesting an enrichment of the *MYOD* and/or *MYOG* combination in the *TMEM8C*+ population. Altogether, we conclude that *TMEM8C* expression essentially correlates with *MYOD*+/*MYOG*+ advanced states of myogenic differentiation.

The fusion marker *TMEM8C* and the myogenic differentiation gene *MYOG* display a regionalised transcript expression within foetal skeletal muscles

In order to compare the spatial location of *TMEM8C* transcripts with those of *MYOD* and *MYOG* within foetal skeletal muscles, we performed in situ hybridization experiments to chicken forelimb adjacent sections at foetal stages. At E6 when the muscle pattern is not yet set, faint *TMEM8C* expression was observed in limb muscle masses, labelled with *MYOD* and *MYOG* transcripts and myosins (Fig. S2). We did not observe any obvious regionalisation of *MYOD* and *MYOG* transcripts within limb muscle masses, labelled with myosins, at this stage (E6) (Fig. S2). At E10, when the musculoskeletal pattern is set, the tendon marker *SCX*, a bHLH transcription factor, was used to label tendons and allow the visualisation of muscle tips (muscle extremities close to tendons) in both longitudinal and transverse limb sections (Fig. 2A,E,I, Fig. S3A-C, G). In situ hybridization experiments to longitudinal (Fig. 2A-H) and transverse (Fig. 2I-L, Fig. S3C-J) muscle sections of E10 chicken embryos showed that *TMEM8C* transcripts were preferentially located in the middle of muscle and less so at muscle tips (Fig. 2B,F,J, Fig. S3D,H). *MYOG* expression was also

higher in the central muscle region compared to muscle tips where the expression was faint (Fig. 2C,G,K, Fig. S3E,I), although *MYOG* expression domain was broader compared to that of *TMEM8C*. In contrast, *MYOD* expression encompassed the entire muscle including muscle tips close to tendons (Fig. 2D,H,L, Fig. S3F,J). These in situ hybridization experiments show that the *TMEM8C* and *MYOG* expression is regionalized, while *MYOD* is homogeneously expressed within foetal muscles.

To confirm the preferential central location of *TMEM8C* transcripts, we compared the expression of *TMEM8C* with that of *FGF4*, known to be expressed in myonuclei at muscle tips close to tendons in limbs (Edom-Vovard et al., 2001, 2002) of chicken embryos. Comparison of *TMEM8C* expression with that of *FGF4* showed a complementary expression pattern, *i.e.* a central muscle location for *TMEM8C* and muscle extremities for *FGF4* (Fig. 3A-D,G,H), while *MYOD* expression (Fig. 3E,F) encompassed the entire muscle. We conclude that the transcripts of *TMEM8C* fusion gene displayed a preferential central location excluded from muscle tips labelled with *FGF4*.

At a cellular level, scRNAseq datasets indicated an exclusion of *TMEM8C* expression from *PAX7*+ progenitors and a preferential expression of *TMEM8C* in *MYOD*+/*MYOG*+ population (Fig. 1). Consistently, double fluorescent in situ hybridisation confirmed that *TMEM8C* expression was excluded from PAX7+ progenitors (Fig. S4A,B,B',B''). We also observed numerous *TMEM8C*+/*MYOD*+ cells and *TMEM8C*+/*MYOG*+ cells within foetal limb muscles (Fig. S4C-F, arrows). Lastly, in central muscle regions *TMEM8C* expression (Fig. S4G,G') was preferentially observed outside myosin+ myotubes (Fig. S4H,H', arrows), although we detected rare myotube expressing *TMEM8C* (Fig. S4H,H', arrowhead). We conclude that the transcripts of *TMEM8C* fusion gene displayed a preferential central location in myogenic cells outside myosin+ myotubes.

MYOG protein is regionalised in foetal muscles

Because of the observed co-segregation of *TMEM8C*+ cells and *MYOG*+ cells in the scRNAseq datasets (Fig. 1) and the regionalised location of *TMEM8C* and *MYOG* transcripts within limb muscles during foetal myogenesis (Figs. 2,3), we investigated the location of the MYOG protein within muscles by immunostaining on limb sections (Fig. 4, Fig. S5). At E6, MYOG+ cells follow a similar pattern of distribution as PAX7+ progenitor cells and myosin+ differentiated cells in dorsal and ventral muscle masses (Fig. S5), which is consistent with the homogeneous *MYOG* transcript distribution (Fig. S2B,B',B"). At E10, when the final muscle pattern is set, muscle tips were visualized with pSMAD1/5/9 antibody (Esteves de Lima et

al., 2021; Wang et al., 2010), while tendons were labelled with collagen type XII. Immunohistochemistry on longitudinal muscle sections showed less MYOG+ nuclei at muscle tips close to tendons, compared to the central muscle regions where MYOG+ cells were more abundant (Fig. 4A-C), consistent with the regionalisation of *MYOG* transcripts (Fig. 2). PAX7+ cells displayed a homogeneous distribution within myosin+ domains (Fig. 4A',A",B'). Immunohistochemistry on transverse sections of a ventro-posterior limb muscle, the FCU (*Flexor Carpi Ulnaris*), further showed the higher density of MYOG+ cells in central muscle regions compared to muscle tips (Fig. 4D,D'), while PAX7+ muscle progenitors (Fig. 4D',E,F') and MYOD+ cells (Fig. 4E) displayed a homogenous distribution within the muscle; the muscle tips being visualized with pSMAD1/5/9+ myonuclei (Fig. 4F,F') close to tendons (Fig. 4G). Quantification of the MYOG+ cells showed a two-fold increase in MYOG+ cell percentage in central regions compared to muscle tips (Fig. 4H-J), with no change in overall DAPI+ nuclei density (Fig. 4K). Conversely, PAX7+ cell percentage was unchanged between the tips and middle muscle domains (Fig. 4J).

We conclude that the transcripts of the fusion marker *TMEM8C* (Figs. 2,3), and the transcripts and protein of the myogenic gene *MYOG* (Fig. 2,4) display a similar and preferential central regionalisation within foetal muscles.

The transcripts of the NOTCH ligand *JAGGED2* are regionalised within limb foetal muscles

The regionalised expression of fusion-associated markers suggested a preferential location of myoblast fusion in central muscle regions. In order to identify signalling pathways that could regulate myoblast fusion, we looked for genes displaying similar regionalisation. Our previous observations suggested a regionalised expression of *JAG2* in limb foetal muscles (see Figure 2A,B in Esteves de Lima et al., 2016). *JAG2* is the main NOTCH ligand produced by myotubes during limb foetal myogenesis in chicken embryos (Delfini et al., 2000; Esteves de Lima et al., 2016). Classical action mode for NOTCH signalling is described as NOTCH ligand being produced by differentiated muscle cells and acting in muscle progenitors (Delfini et al., 2000; Esteves de Lima et al., 2016; Kassar-Duchossoy, 2005; Zalc et al., 2014). Analysis of scRNAseq data sets from limb cells confirmed the expression of the *JAG2* ligand within differentiated muscle cell clusters at E6 and E10, while *HEYL* expression, a readout of NOTCH activity, was associated with the PAX7 progenitor clusters (Fig. 5A,B to be compared with Fig. 1A,D). As expected, cells expressing *JAG2* and *TMEM8C* partially overlap on the contrary to those that express *HEYL* and *TMEM8C* that are mutually exclusive

(Fig. S6A,B,F,G). We confirmed *in vivo* that the NOTCH ligand *JAG2* was regionalised in limb foetal muscles (Fig. 5). *JAG2* transcripts were excluded from muscle tips (Fig. 5D,D',G,G') close to tendons, visualised with *SCX* expression (Fig. 5C,C',F,F'), while *MYOD* transcripts were present homogeneously throughout the muscle (Fig. 5E,E',H,H'). The regionalisation of the NOTCH ligand *JAG2* within muscle fibres suggests a regionalisation of NOTCH activity in the central region of the muscle, where *TMEM8C*+/MYOG+ fusion-competent cells are preferentially located, during foetal myogenesis. As expected from the role of NOTCH signalling as a gate-keeper of myogenesis entry, the fraction of *HEYL*+ cells in myogenic populations decreases with the progression of myogenic differentiation in the scRNAseq data analysis (Fig. 5I, Fig. S6D). Strikingly, within the *MYOD1*+ and/or *MYOG*+ myocyte population, the percentage of *HEYL*+ cells was higher in the *TMEM8C*-negative population versus the fusion-competent *TMEM8C*-positive population (Fig. 5I,J + Fig. S6D ,E, Fig. S6C,H), showing that NOTCH activity and *TMEM8C* expression are mutually exclusive in the differentiated myogenic population. This suggests that down-regulation of NOTCH signalling in differentiated myogenic cells may be required for fusion to occur.

NOTCH loss-of-function increases myoblast fusion in limb foetal muscles

In order to analyse the consequences of NOTCH inhibition on foetal muscle fusion, a dominant-negative form of DELTA1 (DELTA1-DN) under the control of the myosin light chain promoter was overexpressed specifically in differentiated myogenic cells. This prevented NOTCH ligand processing in ligand-producing cells and consequently inhibited NOTCH activation in signal-receiving cells (Chitnis, 2006; Esteves de Lima et al., 2016; Henrique et al., 1997). Limb somite electroporation with such construction increased myoblast fusion (Fig. 6A-C,E-G, arrows indicate examples of Tomato+ fibres), as assessed by the increase in the percentage of myonuclei (MF20+ nuclei) with respect to all nuclei (Fig. 6I) and in the percentage of muscle fibres with a high number of myonuclei compared to control muscles (Fig. 6J). *TMEM8C* expression pattern became wider within the muscle in the NOTCH loss-of-function context compared to controls (Fig. 6D,H). We conclude that NOTCH activity regulates fusion in developing limb muscles.

Chicken embryo immobilisation by DMB (Decamethonium bromide) treatment decreases NOTCH activity and mimics a NOTCH loss-of-function phenotype, *i.e* a reduction in the number of muscle progenitors and increased differentiation; this myogenic phenotype being rescued by NOTCH activation (Esteves de Lima et al., 2016). We used the same

immobilisation condition to further address NOTCH involvement in myoblast fusion in vivo. In contrast to the electroporation technique that leads to a mosaic expression of the electroporated gene within muscle cells, DMB-mediated immobilisation affects all muscles. In immobilisation conditions, following DMB treatment, we observed larger myotubes compared to controls (Fig. 6K,N). We also observed a wider expression pattern of the *TMEM8C* fusion gene within the muscles, associated with the loss of its regionalisation in immobilized embryos compared to controls (Fig. 6L,M,O,P). We further observed the increase of *TMEM8C* mRNA levels by RT-qPCR experiments in immobilized foetal limbs (Fig. 6Q). The increase in the percentage of myonuclei versus all nuclei and in the percentage of muscle fibres with a high number of myonuclei (Fig. 6R,S) confirmed the increased fusion in immobilised embryos compared to controls. The phenotype observed with DMB-mediated immobilisation is consistent with that of NOTCH loss-of-function, albeit stronger, which could be associated with the wider exposure of all muscles to DMB compared to electroporation. To investigate if the DMB-mediated increased fusion could be prevented by forced-NOTCH activity, we performed grafts of DELTA1-expressing cells in one limb of immobilized embryos, using the contralateral limb as control. We observed that the percentage of myonuclei was decreased by DELTA1/DMB limbs compared to DMB limbs only (Fig. S7I-N). This shows that active NOTCH prevents the increased fusion observed in DMB-treated muscles. Taken together, these experiments show that NOTCH loss-of-function conditions increase muscle fusion. Whether this increase in fusion results solely from increased differentiation (Esteves de Lima et al., 2016) or from combined effect on differentiation and fusion cannot be resolved in vivo.

A myoblast culture system that mimics myogenesis

With the ultimate goal to uncouple differentiation and fusion processes, we turned to an in vitro system of chicken foetal myoblast cultures. We first assessed whether cultures of chicken foetal myoblasts mimic in vivo myogenesis. Foetal myoblasts were isolated from limbs of E10 chicken embryos and plated at low density with high serum-containing medium defining proliferation conditions. Muscle cell cultures in proliferation conditions contained PAX7+ progenitor cells and myosin+ differentiated cells (Fig. S8A). When switched to a low serum-containing medium (differentiation conditions), confluent myoblasts were pushed to differentiation and fusion and formed multinucleated myosin+ cells while maintaining a pool of PAX7+ reserve cells (Fig. S8B), as described for mouse myoblast cultures (Baghdadi et al., 2018; Kitzmann et al., 2006). Consistently with the in vivo situation (Bröhl et al., 2012;

Mourikis et al., 2012a), *HEYL* expression was decreased in differentiated muscle cell cultures compared to proliferative myoblast cultures, but still detected in differentiated myoblasts (Fig. S8C). We then performed NOTCH loss- and gain-of-function experiments in proliferative myoblast cultures and compared the phenotypes with those obtained in vivo. We performed NOTCH loss-of-function experiments in myoblasts using the NOTCH inhibitor DAPT. NOTCH inhibition with DAPT increased myoblast differentiation by increasing the expression levels of the differentiation markers *MYOD*, *MYOG* and *MYHC*, while decreasing those of *PAX7* and *MYF5* in proliferative myoblast cultures (Fig. S8D,E,G), consistent with our previous observations (Esteves de Lima et al., 2016). Conversely, we forced NOTCH activity by overexpressing DELTA1 using the RCAS retroviral system in proliferative myoblast cultures and in chicken limbs. DELTA1-activated NOTCH led to the mirror phenotype for myogenesis to that of NOTCH loss-of-function. The expression levels of *MYOD*, *MYOG* and *MYHC* mRNAs were decreased, while those of *PAX7* and *MYF5* were increased in DELTA1-activated NOTCH myoblast cultures (Fig. S7A-H). This is consistent with the decreased expression of *MYOD* and *MYOG* transcripts and the myosin protein, previously described in DELTA1-activated NOTCH limbs of chicken embryos (Bonnet et al., 2010; Delfini et al., 2000). In both NOTCH loss- and gain-of function, the expression of the NOTCH target gene *HEYL* was accordingly dysregulated in myoblasts, while that of the BMP signalling target genes such as *ID1* and *ID2* were not modified (Fig. S8G,H), showing that BMP signalling, previously shown to interact with NOTCH in other systems (Guo and Wang, 2009), is not involved in this process. DELTA1-activated NOTCH increased the percentage of PAX7+ cells in proliferative myoblast cultures (Fig. S8I) and in chicken limbs without increase in muscle area after two days of DELTA1/RCAS exposure (Fig. S7A-H) compared to respective controls. These results combined with literature data show that cultures of chicken foetal myoblasts mimic in vivo myogenesis and that NOTCH loss- and gain-of-function lead to similar outcomes for muscle differentiation in vivo and in vitro.

NOTCH loss-of-function in differentiating myoblast cultures increases terminal differentiation and fusion

In order to assess the effect of NOTCH inhibition on the later steps of myogenesis, DAPT-mediated NOTCH loss-of function was performed on differentiating myoblast cultures (Fig. 7A-E). DAPT-mediated NOTCH inhibition favoured the appearance of myotubes and a decrease in the percentage of PAX7+ cells compared to controls, with no change in the nuclei number (Fig. 7A-C). Consistently, the expression of the muscle differentiation markers

MYOG and *MYHC* was increased, while that of *PAX7* was decreased, in DAPT-treated cultures compared to control cultures (Fig. 7D). *TMEM8C* expression was also increased in DAPT-treated cultures, while the NOTCH target gene *HEYL* was downregulated (Fig. 7D). Consistent with the increase of *TMEM8C* and *MYHC* mRNA levels (Fig. 7D), the myotubes were larger (Fig. 7A,B) and the fusion index was significantly increased in DAPT-treated differentiating myoblast cultures compared to controls (Fig. 7E). These results show that NOTCH inhibition increases the terminal differentiation and fusion processes in foetal myoblasts cultured in differentiation conditions.

NOTCH loss-of-function in differentiated MYOG+ myoblasts increases fusion

In the previous NOTCH inhibition experiments (Fig. 7A-E), we could not dissociate muscle cell differentiation from fusion. In order to uncouple differentiation from fusion, we used a two-step protocol where proliferating myoblasts were first pushed to differentiate without fusion and then allowed to fuse in a second step (Fig. 7F). Based on previously described protocols (Girardi et al., 2021; Latroche et al., 2017), we induced differentiation of myoblasts, seeded at a sub-confluent concentration to avoid cell-cell contact and thereby fusion, by culturing them in a low serum-containing medium (Fig. 7F). As expected, after this procedure, myoblasts lost PAX7 expression and became MYOG+ (Fig. 7G-I). MYOG+ differentiated myoblasts (myocytes) were then plated at high density and treated with either DAPT or DMSO for 48 hours to assess the effect of NOTCH inhibition on the fusion process of already-differentiated myoblasts (Fig. 7F). DAPT-mediated NOTCH inhibition favoured myotube formation compared to controls (Fig. 7J,K). The fusion index was significantly increased in the context of NOTCH inhibition compared to control cultures (Fig. 7L). Consistently, the expression of *TMEM8C* increased with DAPT exposure, while the expression of *MYOD* and *MYOG* did not significantly increase compared to controls in this two-step-culture system (Fig. S9). Taken together, these results show that NOTCH inhibition in differentiated myoblasts promotes fusion independently from differentiation in vitro.

HEYL binds to the promoter regions of *TMEM8C* in chick limbs and myoblast cultures

In order to define the molecular mechanism through which NOTCH inhibition promoted myoblast fusion, we analysed the recruitment of the NOTCH target gene HEYL to the *TMEM8C* promoter regions previously described (Luo et al., 2015). Because the HEY/HES are bHLH transcriptional repressors known to inhibit myogenesis via the direct binding to E-boxes-containing regions of the *MYOD* enhancer (Zalc et al., 2014), we tested if HEYL could

bind to the 3 E-boxes-containing regions in regulatory regions of the *TMEM8C* fusion gene (Fig. 8A). In order to test this hypothesis, we performed chromatin immunoprecipitation (ChIP) experiments in samples from DAPT-treated cultures of differentiated myoblasts (two-step protocol) and immobilised limbs (as the phenotype observed with DMB was similar but stronger than that following DELTA1-DN electroporation). We found that in the control for both the myoblast culture and the limb, the transcriptional repressor HEYL was recruited to the 3 E-box-containing regions located upstream of *TMEM8C* gene (Fig. 8B,C). In addition, NOTCH inhibition led to decreased binding of HEYL to these regions compared to control conditions (Fig. 8B,C). This result is consistent with the increase in *TMEM8C* expression and fusion index in the DAPT-treated myoblast cultures (Fig. 7) and in NOTCH loss-of-function experiments on limb foetal muscles (Fig. 6). The decrease of HEYL recruitment to the *TMEM8C* promoter in the absence of NOTCH activity in vivo and in vitro provides a potential mechanism for the fusion-inhibiting effect of NOTCH signalling pathway (Fig. 8D).

Discussion

In the present study we identified a regionalised location for the *TMEM8C* fusion gene transcripts and for the fusion-competent MYOG+ cells in limb foetal muscles of chicken embryos and established a molecular link between the NOTCH pathway and *TMEM8C* expression that could underlie the fusion-inhibiting effect of NOTCH.

Whether the fusion process occurs at specific places within the skeletal muscles is not known. We identified a preferential central location for *TMEM8C* transcripts and fusion-competent MYOG+ cells in skeletal muscles during foetal myogenesis in chicken (Fig. 8E). The similar location of MYOG+ cells and *TMEM8C* transcripts is fully consistent with the transcriptional regulation of *TMEM8C* expression by MYOG (Ganassi et al., 2018; Luo et al., 2015; Millay et al., 2013). This regionalized expression suggests that fusion would preferentially occur in the central region of the muscle during chicken foetal development. Because Myomaker/TMEM8C is required in both fusing cells (Millay et al., 2013) and *TMEM8C* is preferentially expressed in fusion-competent cells outside muscle fibres (Fig. S4), two scenarii for fusion are possible. In the first, mononucleated fusion-competent cells fuse to form de novo fibres. In the second, mononucleated fusion-competent cells fuse to existing fibres that rapidly downregulate TMEM8C expression.

In apparent contradiction, based on BrdU incorporation experiments, myoblast fusion has been suggested to occur preferentially at muscle tips in rat and mouse muscles during foetal and perinatal growth (Gu et al., 2016; Kitiyakara and Angevine, 1963; Zhang and McLennan, 1995). However, these BrdU incorporation experiments did not address specifically myoblast fusion, but rather cell fusion. One cannot exclude that these BrdU experiments revealed fibroblast fusion preferentially at muscle tips, since fibroblasts can be recruited to the myogenic fate at the muscle-tendon interface (Esteves de Lima et al., 2021; Yaseen et al., 2021). Furthermore, it has been shown a preferential location of proliferating PAX7+ cells at muscle tips close to tendons, indicating that the muscle-tendon environment favours a proliferative state of the myoblasts rather than myoblast differentiation and fusion (Esteves de Lima et al., 2014).

Because NOTCH inhibition is a potent trigger of muscle differentiation, the role of NOTCH in muscle fusion has been neglected. We show now that the expression of the NOTCH ligand *JAG2* is preferentially localised in the central muscle regions and excluded from the tips (Fig. 8E), which compares to the regionalisation observed for the MYOG+ cells and *TMEM8C* transcripts. We further demonstrate that NOTCH inhibition increased myoblast fusion in addition to differentiation in foetal myoblast cultures and limb muscles. These results suggest that the endogenous levels of *JAG2* in the central muscle regions are potentially required to regulate the NOTCH ON (HEYL+) and NOTCH OFF (HEYL-) states in differentiated myoblasts (Fig. 5, Fig. S6) and consequently the flux of fusion events in this zone. This is consistent with the myotube hypertrophy observed in mouse C2.7 myoblasts upon NOTCH inhibition (Kitzmann et al., 2006). Many of the molecules identified as being involved in myoblast fusion can be linked to NOTCH signalling. The calcium-activated transcription factor NFATC2, recognized to control myoblast fusion after the initial formation of myotubes (Horsley et al., 2003), has the ability to suppress NOTCH transactivation and the expression of *Hey* genes (Zanotti et al., 2013). Shisa2, an endoplasmic reticulum (ER) localized protein that regulates the fusion of mouse myoblasts via Rac1/Cdc42-mediated cytoskeletal F-actin remodelling, is repressed by NOTCH signalling (Liu et al., 2018). SRF that was identified as a regulator of satellite cell fusion via the maintenance of actin cytoskeleton architecture (Randrianarison-Huetz et al., 2018), physically interacts with the NOTCH target gene Herp1 that interferes with SRF transcriptional activity (Doi et al., 2005). Recently, it has been reported that TGFβ inhibition promotes muscle cell fusion in chicken embryos and adult mouse muscles by modulating actin dynamics (Girardi et al., 2021; Melendez et al., 2021). Interestingly, crosstalks have been identified between TGFβ and NOTCH intracellular

signalling pathways, which lead to functional synergism for both pathways. TGFβ cooperates with NOTCH to induce *Hes1*, *Hey1* and *Jag1* expression in a Smad3-dependent manner through a Smad3–NICD interaction in different systems (Blokzijl, 2003; Zavadil et al., 2004). Given this positive interaction, we cannot exclude that TGFβ inhibition interferes with NOTCH signalling or vice versa during myoblast fusion. NOTCH decay has been also involved in the fusion of fusion-competent myoblasts into myotubes in adult Drosophila (Gildor et al., 2012), suggesting a conserved involvement of NOTCH inhibition in myoblast fusion in invertebrates and vertebrates.

In addition to showing a fusion-inhibiting effect of NOTCH in vertebrates, we established a molecular link between *HEYL* and the fusion gene *TMEM8C* (*Myomaker*). In control conditions, the recruitment of the HEYL transcriptional repressor to the E-box-containing regions of the *TMEM8C* promoter could potentially be the basis for the absence of fusion ability of muscle progenitors displaying active NOTCH. In the context of NOTCH inhibition, the expression of *HEYL* is decreased and consequently HEYL recruitment to *TMEM8C* promoter regions is lost, which results in the release of the inhibition of *TMEM8C* expression (Fig. 8D). The increase of *TMEM8C* expression is likely to be the molecular mechanism underlying the increased fusion observed in NOTCH inhibition conditions. This also indicates that during normal development, when NOTCH activity is decreased in muscle cells, muscle fusion is promoted in addition to differentiation. The myogenic differentiation factors MYOD/MYOG also bind to the E-box domain located close to the transcription start site of *Myomaker* to positively regulate its expression in mouse (*Mymk*), chicken (*TMEM8C)* and zebrafish (*mymk*) (Ganassi et al., 2018; Luo et al., 2015; Millay et al., 2014). One attractive mechanism could be a competition between HEYL transcriptional repressor and MYOG transcriptional activator for the occupancy of the *TMEM8C* promoter regions. In the context of active NOTCH, MYOG is not present and HEYL represses *TMEM8C* transcription, while in the context of NOTCH inhibition, HEYL is decreased and MYOG is present and activates *TMEM8C* transcription. This provides a possible new mechanism for tuning myoblast differentiation and fusion during development.

Acknowledgements

We thank lab members, Matthew Borok, Philippos Mourikis, Sonya Nassari and Valentina Taglietti for critical reading of the MS. We thank So-Ichiro Fukada, Manuel Koch and Christophe Marcelle for reagents. We thank Sophie Gournet for illustrations.

Competing interests

No competing interests declared.

Funding

The work was supported by the AFM MyoSig N°15761, AFM Myoconnect N°16752, ANR-20-CE13-0020-01, FRM DEQ20140329500 and CNRS, UPMC, INSERM. JEdL was part of the MyoGrad International Research Training Group for Myology and was supported by the DFG and the AFM. JEdL was then supported by a Labex REVIVE post-doctoral fellowship.

References

Andersson, E.R., Sandberg, R., and Lendahl, U. (2011). Notch signaling: simplicity in design, versatility in function. Development *138*, 3593–3612.

Baghdadi, M.B., Castel, D., Machado, L., Fukada, S., Birk, D.E., Relaix, F., Tajbakhsh, S., and Mourikis, P. (2018). Reciprocal signalling by Notch–Collagen V–CALCR retains muscle stem cells in their niche. Nature *557*, 714–718.

Bi, P., Ramirez-Martinez, A., Li, H., Cannavino, J., McAnally, J.R., Shelton, J.M., Sánchez-Ortiz, E., Bassel-Duby, R., and Olson, E.N. (2017). Control of muscle formation by the fusogenic micropeptide myomixer. Science *356*, 323–327.

Biressi, S., Molinaro, M., and Cossu, G. (2007). Cellular heterogeneity during vertebrate skeletal muscle development. Dev. Biol. *308*, 281–293.

Bjornson, C.R.R., Cheung, T.H., Liu, L., Tripathi, P.V., Steeper, K.M., and Rando, T.A. (2012). Notch signaling is necessary to maintain quiescence in adult muscle stem cells. Stem Cells Dayt. Ohio *30*, 232–242.

Blokzijl, A. (2003). Cross-talk between the Notch and TGF- signaling pathways mediated by interaction of the Notch intracellular domain with Smad3. J. Cell Biol. *163*, 723–728.

Bonnet, A., Dai, F., Brand-Saberi, B., and Duprez, D. (2010). Vestigial-like 2 acts downstream of MyoD activation and is associated with skeletal muscle differentiation in chick myogenesis. Mech. Dev. *127*, 120–136.

Bourgeois, A., Esteves de Lima, J., Charvet, B., Kawakami, K., Stricker, S., and Duprez, D. (2015). Stable and bicistronic expression of two genes in somite- and lateral plate-derived tissues to study chick limb development. BMC Dev. Biol. *15*, 39.

Bröhl, D., Vasyutina, E., Czajkowski, M.T., Griger, J., Rassek, C., Rahn, H.-P., Purfürst, B., Wende, H., and Birchmeier, C. (2012). Colonization of the Satellite Cell Niche by Skeletal Muscle Progenitor Cells Depends on Notch Signals. Dev. Cell *23*, 469–481.

Buckingham, M., and Rigby, P.W.J. (2014). Gene Regulatory Networks and Transcriptional Mechanisms that Control Myogenesis. Dev. Cell *28*, 225–238.

Chitnis, A. (2006). Why is delta endocytosis required for effective activation of notch? Dev. Dyn. *235*, 886–894.

Comai, G., and Tajbakhsh, S. (2014). Molecular and cellular regulation of skeletal myogenesis. Curr. Top. Dev. Biol. *110*, 1–73.

Conboy, I.M., and Rando, T.A. (2002). The regulation of Notch signaling controls satellite cell activation and cell fate determination in postnatal myogenesis. Dev. Cell *3*, 397–409.

Conboy, I.M., Conboy, M.J., Smythe, G.M., and Rando, T.A. (2003). Notch-mediated restoration of regenerative potential to aged muscle. Science *302*, 1575–1577.

Conboy, I.M., Conboy, M.J., Wagers, A.J., Girma, E.R., Weissman, I.L., and Rando, T.A. (2005). Rejuvenation of aged progenitor cells by exposure to a young systemic environment. Nature *433*, 760–764.

Conway, J.R., Lex, A., and Gehlenborg, N. (2017). UpSetR: an R package for the visualization of intersecting sets and their properties. Bioinformatics *33*, 2938–2940.

Delfini, M.-C., and Duprez, D. (2004). Ectopic Myf5 or MyoD prevents the neuronal differentiation program in addition to inducing skeletal muscle differentiation, in the chick neural tube. Dev. Camb. Engl. *131*, 713–723.

Delfini, M., Hirsinger, E., Pourquié, O., and Duprez, D. (2000). Delta 1-activated notch inhibits muscle differentiation without affecting Myf5 and Pax3 expression in chick limb myogenesis. Development *127*, 5213–5224.

Di Gioia, S.A., Connors, S., Matsunami, N., Cannavino, J., Rose, M.F., Gilette, N.M., Artoni, P., de Macena Sobreira, N.L., Chan, W.-M., Webb, B.D., et al. (2017). A defect in myoblast fusion underlies Carey-Fineman-Ziter syndrome. Nat. Commun. *8*, 16077.

Doi, H., Iso, T., Yamazaki, M., Akiyama, H., Kanai, H., Sato, H., Kawai-Kowase, K., Tanaka, T., Maeno, T., Okamoto, E., et al. (2005). HERP1 inhibits myocardin-induced vascular smooth muscle cell differentiation by interfering with SRF binding to CArG box. Arterioscler. Thromb. Vasc. Biol. *25*, 2328–2334.

Duprez, D. (2002). Signals regulating muscle formation in the limb during embryonic development. Int. J. Dev. Biol. *46*, 915–926.

Edom-Vovard, F., Bonnin, M.-A., and Duprez, D. (2001). Misexpression of Fgf-4 in the Chick Limb Inhibits Myogenesis by Down-Regulating Frek Expression. Dev. Biol. *233*, 56–71.

Edom-Vovard, F., Schuler, B., Bonnin, M.-A., Teillet, M.-A., and Duprez, D. (2002). Fgf4 positively regulates scleraxis and tenascin expression in chick limb tendons. Dev. Biol. *247*, 351–366.

Esteves de Lima, J., and Relaix, F. (2021). Master regulators of skeletal muscle lineage development and pluripotent stem cells differentiation. Cell Regen. *10*, 31.

Esteves de Lima, J., Bonnin, M.-A., Bourgeois, A., Parisi, A., Le Grand, F., and Duprez, D. (2014). Specific pattern of cell cycle during limb fetal myogenesis. Dev. Biol. *392*, 308–323.

Esteves de Lima, J., Bonnin, M.-A., Birchmeier, C., and Duprez, D. (2016). Muscle contraction is required to maintain the pool of muscle progenitors via YAP and NOTCH during fetal myogenesis. ELife *5*, e15593.

Esteves de Lima, J., Blavet, C., Bonnin, M.-A., Hirsinger, E., Comai, G., Yvernogeau, L., Delfini, M.-C., Bellenger, L., Mella, S., Nassari, S., et al. (2021). Unexpected contribution of fibroblasts to muscle lineage as a mechanism for limb muscle patterning. Nat. Commun. *12*, 3851.

Fukada, S., Uezumi, A., Ikemoto, M., Masuda, S., Segawa, M., Tanimura, N., Yamamoto, H., Miyagoe-Suzuki, Y., and Takeda, S. (2007). Molecular signature of quiescent satellite cells in adult skeletal muscle. Stem Cells Dayt. Ohio *25*, 2448–2459.

Fukada, S. -i., Yamaguchi, M., Kokubo, H., Ogawa, R., Uezumi, A., Yoneda, T., Matev, M.M., Motohashi, N., Ito, T., Zolkiewska, A., et al. (2011). Hesr1 and Hesr3 are essential to generate undifferentiated quiescent satellite cells and to maintain satellite cell numbers. Development *138*, 4609–4619.

Ganassi, M., Badodi, S., Ortuste Quiroga, H.P., Zammit, P.S., Hinits, Y., and Hughes, S.M. (2018). Myogenin promotes myocyte fusion to balance fibre number and size. Nat. Commun. *9*, 4232.

Gildor, B., Schejter, E.D., and Shilo, B.-Z. (2012). Bidirectional Notch activation represses fusion competence in swarming adult Drosophila myoblasts. Dev. Camb. Engl. *139*, 4040–4050.

Girardi, F., Taleb, A., Ebrahimi, M., Datye, A., Gamage, D.G., Peccate, C., Giordani, L., Millay, D.P., Gilbert, P.M., Cadot, B., et al. (2021). TGFβ signaling curbs cell fusion and muscle regeneration. Nat. Commun. *12*, 750.

Gu, J.-M., Wang, D.J., Peterson, J.M., Shintaku, J., Liyanarachchi, S., Coppola, V., Frakes, A.E., Kaspar, B.K., Cornelison, D.D., and Guttridge, D.C. (2016). An NF-κB--EphrinA5-Dependent Communication between NG2(+) Interstitial Cells and Myoblasts Promotes Muscle Growth in Neonates. Dev. Cell *36*, 215–224.

Guo, X., and Wang, X.-F. (2009). Signaling cross-talk between TGF-β/BMP and other pathways. Cell Res. *19*, 71–88.

Harada, A., Maehara, K., Ono, Y., Taguchi, H., Yoshioka, K., Kitajima, Y., Xie, Y., Sato, Y., Iwasaki, T., Nogami, J., et al. (2018). Histone H3.3 sub-variant H3mm7 is required for normal skeletal muscle regeneration. Nat. Commun. *9*, 1400.

Havis, E., Anselme, I., and Schneider-Maunoury, S. (2006). Whole embryo chromatin immunoprecipitation protocol for the in vivo study of zebrafish development. BioTechniques *40*, 34–40.

Havis, E., Coumailleau, P., Bonnet, A., Bismuth, K., Bonnin, M.-A., Johnson, R., Fan, C.-M., Relaix, F., Shi, D.-L., and Duprez, D. (2012). Sim2 prevents entry into the myogenic program by repressing MyoD transcription during limb embryonic myogenesis. Development *139*, 1910–1920.

Henrique, D., Hirsinger, E., Adam, J., Roux, I.L., Pourquié, O., Ish-Horowicz, D., and Lewis, J. (1997). Maintenance of neuroepithelial progenitor cells by Delta–Notch signalling in the embryonic chick retina. Curr. Biol. *7*, 661–670.

Hernández, J.M., and Podbilewicz, B. (2017). The hallmarks of cell-cell fusion. Dev. Camb. Engl. *144*, 4481–4495.

Hirsinger, E., Malapert, P., Dubrulle, J., Delfini, M.-C., Duprez, D., Henrique, D., Ish-Horowicz, D., and Pourquié, O. (2001). Notch signalling acts in postmitotic avian myogenic cells to control MyoD activation. Development *128*, 107–116.

Horsley, V., Jansen, K.M., Mills, S.T., and Pavlath, G.K. (2003). IL-4 acts as a myoblast recruitment factor during mammalian muscle growth. Cell *113*, 483–494.

Kassar-Duchossoy, L. (2005). Pax3/Pax7 mark a novel population of primitive myogenic cells during development. Genes Dev. *19*, 1426–1431.

Kim, J.H., Jin, P., Duan, R., and Chen, E.H. (2015). Mechanisms of myoblast fusion during muscle development. Curr. Opin. Genet. Dev. *32*, 162–170.

Kitiyakara, A., and Angevine, D.M. (1963). A STUDY OF THE PATTERN OF POSTEMBRYONIC GROWTH OF M. GRACILIS IN MICE. Dev. Biol. *8*, 322–340.

Kitzmann, M., Bonnieu, A., Duret, C., Vernus, B., Barro, M., Laoudj-Chenivesse, D., Verdi, J.M., and Carnac, G. (2006). Inhibition of Notch signaling induces myotube hypertrophy by recruiting a subpopulation of reserve cells. J. Cell. Physiol. *208*, 538–548.

Koch, M., Bernasconi, C., and Chiquet, M. (1992). A major oligomeric fibroblast proteoglycan identified as a novel large form of type-XII collagen. Eur. J. Biochem. *207*, 847–856.

Kopan, R., Nye, J.S., and Weintraub, H. (1994). The intracellular domain of mouse Notch: a constitutively activated repressor of myogenesis directed at the basic helix-loop-helix region of MyoD. Development *120*, 2385–2396.

Kuroda, K., Tani, S., Tamura, K., Minoguchi, S., Kurooka, H., and Honjo, T. (1999). Delta-induced Notch signaling mediated by RBP-J inhibits MyoD expression and myogenesis. J. Biol. Chem. *274*, 7238–7244.

Lahmann, I., Bröhl, D., Zyrianova, T., Isomura, A., Czajkowski, M.T., Kapoor, V., Griger, J., Ruffault, P.-L., Mademtzoglou, D., Zammit, P.S., et al. (2019). Oscillations of MyoD and Hes1 proteins regulate the maintenance of activated muscle stem cells. Genes Dev. *33*, 524–535.

Landemaine, A., Rescan, P.-Y., and Gabillard, J.-C. (2014). Myomaker mediates fusion of fast myocytes in zebrafish embryos. Biochem. Biophys. Res. Commun. *451*, 480–484.

Latroche, C., Weiss-Gayet, M., Muller, L., Gitiaux, C., Leblanc, P., Liot, S., Ben-Larbi, S., Abou-Khalil, R., Verger, N., Bardot, P., et al. (2017). Coupling between Myogenesis and Angiogenesis during Skeletal Muscle Regeneration Is Stimulated by Restorative Macrophages. Stem Cell Rep. *9*, 2018–2033.

Liu, Z., Wang, C., Liu, X., and Kuang, S. (2018). Shisa2 regulates the fusion of muscle progenitors. Stem Cell Res. *31*, 31–41.

Livak, K.J., and Schmittgen, T.D. (2001). Analysis of relative gene expression data using real-time quantitative PCR and the 2(-Delta Delta C(T)) Method. Methods San Diego Calif *25*, 402–408.

Lubman, O.Y., Ilagan, M.X.G., Kopan, R., and Barrick, D. (2007). Quantitative dissection of the Notch:CSL interaction: insights into the Notch-mediated transcriptional switch. J. Mol. Biol. *365*, 577–589.

Luo, W., Li, E., Nie, Q., and Zhang, X. (2015). Myomaker, Regulated by MYOD, MYOG and miR-140-3p, Promotes Chicken Myoblast Fusion. Int. J. Mol. Sci. *16*, 26186–26201.

Macosko, E.Z., Basu, A., Satija, R., Nemesh, J., Shekhar, K., Goldman, M., Tirosh, I., Bialas, A.R., Kamitaki, N., Martersteck, E.M., et al. (2015). Highly Parallel Genome-wide Expression Profiling of Individual Cells Using Nanoliter Droplets. Cell *161*, 1202–1214.

Manceau, M., Gros, J., Savage, K., Thome, V., McPherron, A., Paterson, B., and Marcelle, C. (2008). Myostatin promotes the terminal differentiation of embryonic muscle progenitors. Genes Dev. *22*, 668–681.

Melendez, J., Sieiro, D., Salgado, D., Morin, V., Dejardin, M.-J., Zhou, C., Mullen, A.C., and Marcelle, C. (2021). TGFβ signalling acts as a molecular brake of myoblast fusion. Nat. Commun. *12*, 749.

Millay, D.P., O'Rourke, J.R., Sutherland, L.B., Bezprozvannaya, S., Shelton, J.M., Bassel-Duby, R., and Olson, E.N. (2013). Myomaker is a membrane activator of myoblast fusion and muscle formation. Nature *499*, 301–305.

Millay, D.P., Sutherland, L.B., Bassel-Duby, R., and Olson, E.N. (2014). Myomaker is essential for muscle regeneration. Genes Dev. *28*, 1641–1646.

Millay, D.P., Gamage, D.G., Quinn, M.E., Min, Y.-L., Mitani, Y., Bassel-Duby, R., and Olson, E.N. (2016). Structure-function analysis of myomaker domains required for myoblast fusion. Proc. Natl. Acad. Sci. U. S. A. *113*, 2116–2121.

Mourikis, P., Gopalakrishnan, S., Sambasivan, R., and Tajbakhsh, S. (2012a). Cell-autonomous Notch activity maintains the temporal specification potential of skeletal muscle stem cells. Development *139*, 4536–4548.

Mourikis, P., Sambasivan, R., Castel, D., Rocheteau, P., Bizzarro, V., and Tajbakhsh, S. (2012b). A Critical Requirement for Notch Signaling in Maintenance of the Quiescent Skeletal Muscle Stem Cell State. STEM CELLS *30*, 243–252.

Noguchi, Y.-T., Nakamura, M., Hino, N., Nogami, J., Tsuji, S., Sato, T., Zhang, L., Tsujikawa, K., Tanaka, T., Izawa, K., et al. (2019). Cell-autonomous and redundant roles of Hey1 and HeyL in muscle stem cells: HeyL requires Hes1 to bind diverse DNA sites. Dev. Camb. Engl. *146*.

Quinn, M.E., Goh, Q., Kurosaka, M., Gamage, D.G., Petrany, M.J., Prasad, V., and Millay, D.P. (2017). Myomerger induces fusion of non-fusogenic cells and is required for skeletal muscle development. Nat. Commun. *8*, 15665.

Randrianarison-Huetz, V., Papaefthymiou, A., Herledan, G., Noviello, C., Faradova, U., Collard, L., Pincini, A., Schol, E., Decaux, J.F., Maire, P., et al. (2018). Srf controls satellite cell fusion through the maintenance of actin architecture. J. Cell Biol. *217*, 685–700.

Schmittgen, T.D., and Livak, K.J. (2008). Analyzing real-time PCR data by the comparative C T method. Nat. Protoc. *3*, 1101–1108.

Schneider, C.A., Rasband, W.S., and Eliceiri, K.W. (2012). NIH Image to ImageJ: 25 years of image analysis. Nat. Methods *9*, 671–675.

Schuster-Gossler, K., Cordes, R., and Gossler, A. (2007). Premature myogenic differentiation and depletion of progenitor cells cause severe muscle hypotrophy in Delta1 mutants. Proc. Natl. Acad. Sci. U. S. A. *104*, 537–542.

Stuart, T., Butler, A., Hoffman, P., Hafemeister, C., Papalexi, E., Mauck, W.M., Hao, Y., Stoeckius, M., Smibert, P., and Satija, R. (2019). Comprehensive Integration of Single-Cell Data. Cell *177*, 1888-1902.e21.

Vasyutina, E., Lenhard, D.C., Wende, H., Erdmann, B., Epstein, J.A., and Birchmeier, C. (2007). RBP-J (Rbpsuh) is essential to maintain muscle progenitor cells and to generate satellite cells. Proc. Natl. Acad. Sci. *104*, 4443–4448.

Wang, H., Noulet, F., Edom-Vovard, F., Le Grand, F., and Duprez, D. (2010). Bmp Signaling at the Tips of Skeletal Muscles Regulates the Number of Fetal Muscle Progenitors and Satellite Cells during Development. Dev. Cell *18*, 643–654.

Wang, H., Bonnet, A., Delfini, M.C., Kawakami, K., Takahashi, Y., and Duprez, D. (2011). Stable, conditional, and muscle-fiber-specific expression of electroporated transgenes in chick limb muscle cells. Dev. Dyn. *240*, 1223–1232.

Weintraub, H., Dwarki, V.J., Verma, I., Davis, R., Hollenberg, S., Snider, L., Lassar, A., and Tapscott, S.J. (1991). Muscle-specific transcriptional activation by MyoD. Genes Dev. *5*, 1377–1386.

Wickham, H. (2016). ggplot2: Elegant Graphics for Data Analysis (New York, NY: Springer).

Wilmerding, A., Rinaldi, L., Caruso, N., Lo Re, L., Bonzom, E., Saurin, A.J., Graba, Y., and Delfini, M.-C. (2021). HoxB genes regulate neuronal delamination in the trunk neural tube by controlling the expression of Lzts1. Development *148*, dev195404.

Yaseen, W., Kraft-Sheleg, O., Zaffryar-Eilot, S., Melamed, S., Sun, C., Millay, D.P., and Hasson, P. (2021). Fibroblast fusion to the muscle fiber regulates myotendinous junction formation. Nat. Commun. *12*, 3852.

Zalc, A., Hayashi, S., Aurade, F., Brohl, D., Chang, T., Mademtzoglou, D., Mourikis, P., Yao, Z., Cao, Y., Birchmeier, C., et al. (2014). Antagonistic regulation of p57kip2 by Hes/Hey downstream of Notch signaling and muscle regulatory factors regulates skeletal muscle growth arrest. Development *141*, 2780–2790.

Zanotti, S., Smerdel-Ramoya, A., and Canalis, E. (2013). Nuclear factor of activated T-cells (NFAT)C2 inhibits Notch receptor signaling in osteoblasts. J. Biol. Chem. *288*, 624–632.

Zavadil, J., Cermak, L., Soto-Nieves, N., and Böttinger, E.P. (2004). Integration of TGF-beta/Smad and Jagged1/Notch signalling in epithelial-to-mesenchymal transition. EMBO J. *23*, 1155–1165.

Zhang, M., and McLennan, I.S. (1995). During secondary myotube formation, primary myotubes preferentially absorb new nuclei at their ends. Dev. Dyn. Off. Publ. Am. Assoc. Anat. *204*, 168–177.

Zhang, Q., Vashisht, A.A., O'Rourke, J., Corbel, S.Y., Moran, R., Romero, A., Miraglia, L., Zhang, J., Durrant, E., Schmedt, C., et al. (2017). The microprotein Minion controls cell fusion and muscle formation. Nat. Commun. *8*, 15664.

Figures

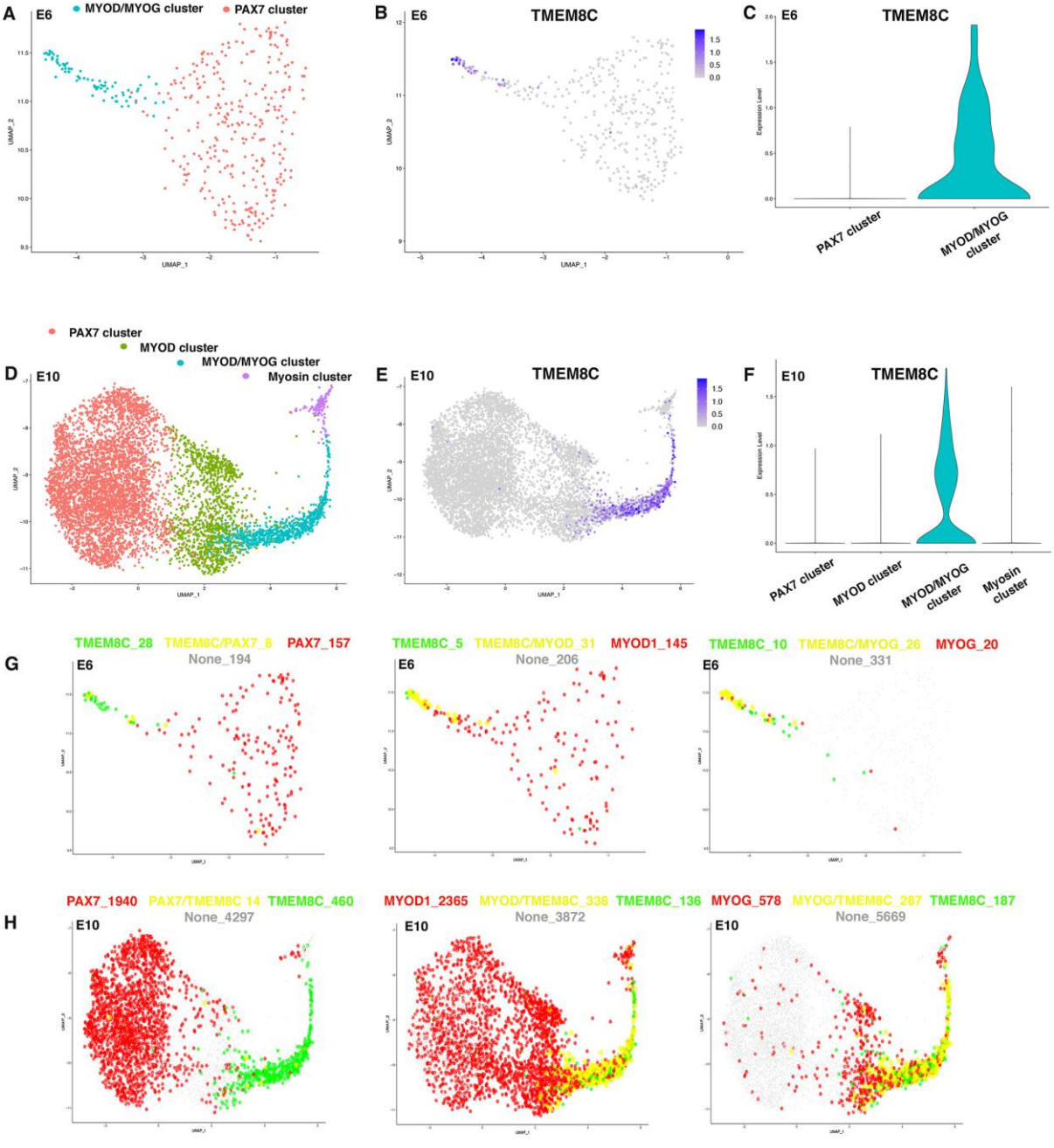

I

	Percentage of TMEM8C+ cells in gene+ population	
Gene+ population	**E6**	**E10**
PAX7+ population	4,8	0,7
MYOD+ population	17,6	12,5
MYOG+ population	56,5	33,2

	Percentage of gene+ cells in TMEM8C+ population	
Gene+ cells	**E6**	**E10**
PAX7+ cells	22,2	2,9
MYOD+ cells	86,1	71,3
MYOG+ cells	72,2	60,5

Figure 1. *TMEM8C* is co-expressed with *MYOD* and *MYOG* in limb foetal muscles

(**A**) UMAP plot showing the distribution of the 2 muscle clusters, PAX7 and MYOD/MYOG clusters at E6. (**B**) Feature plot showing the distribution of *TMEM8C*+ cells across muscle clusters at E6. (**C**) Violin plot showing Log-normalized expression levels of the *TMEM8C* gene in cells grouped by muscle clusters at E6. (**D**) UMAP plot showing the distribution of the 4 muscle clusters, PAX7, MYOD, MYOD/MYOG and Myosin clusters at E10. (**E**) Feature plot showing the distribution of *TMEM8C*+ cells across muscle clusters at E10. (**F**) Violin plot showing Log-normalized expression levels of the *TMEM8C* gene in cells grouped by muscle clusters at E10. (**G,H**) Feature plots showing the distribution of *TMEM8C*+ cells (green dots), *Myogenic marker*+ cells (red dots) and double *TMEM8C*+/*Myogenic marker* + cells (yellow dots) within the muscle clusters at E6 (G) and E10 (H). The following double combinations were analysed: *PAX7+/TMEM8C*+ (left panels), *MYOD+/TMEM8C*+ (middle panels) and *MYOG+/TMEM8C*+ (right panels). (**I**) Upper panel: percentage of *PAX7*+, *MYOD*+ or *MYOG*+ cells among the *TMEM8C*+ cell population at E6 and E10. Lower panel: percentage of *TMEM8C*+ cells among the *PAX7*+, *MYOD*+ or *MYOG*+ cell population at E6 and E10. Numbers used for percentage calculations are those of panels G and H.

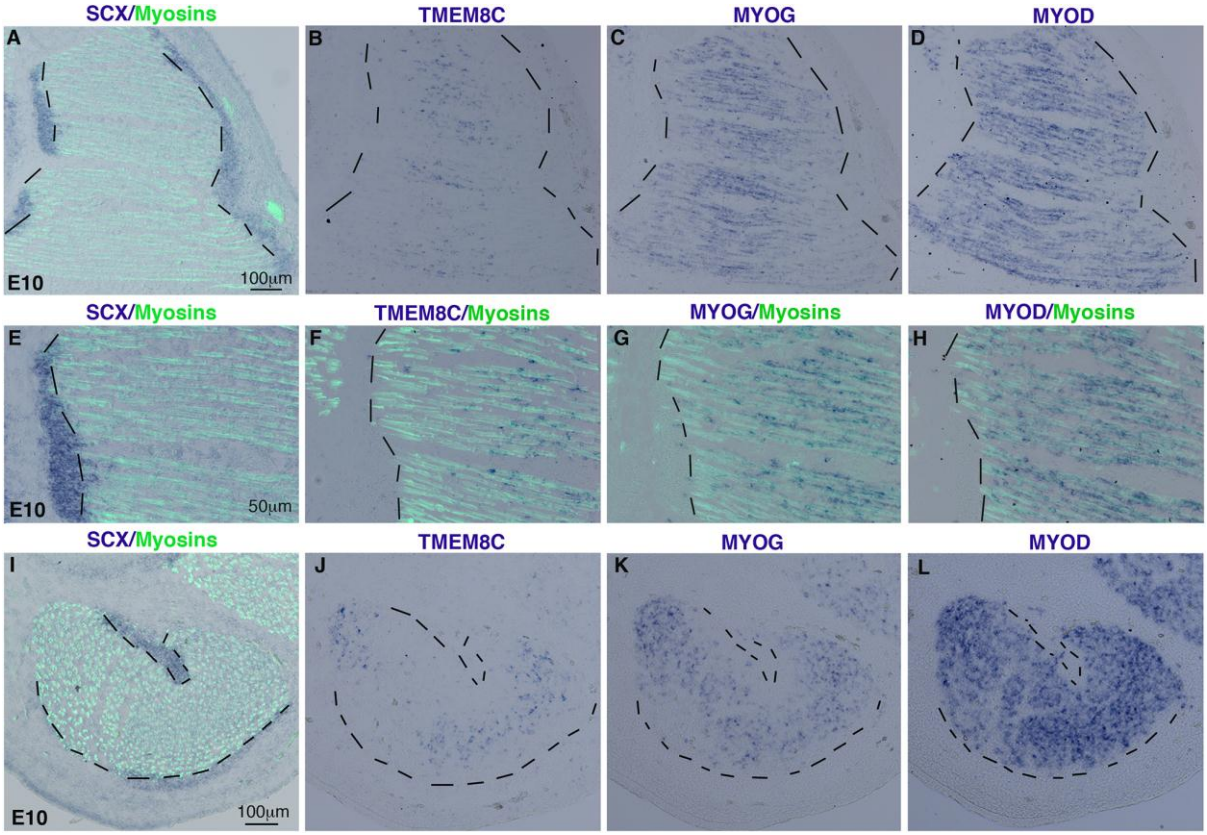

Figure 2. *TMEM8C* transcripts are regionalized in foetal skeletal muscles of E10 chicken limbs

(**A-H**) In situ hybridization to adjacent and longitudinal muscle sections of E10 chicken embryos with the SCX (A,E), TMEM8C (B,F), MYOG (C,G) and MYOD (D,H) probes, followed by immunohistochemistry with the MF20 antibody to visualize myosins (n=4 embryos) (A, E-H). (A,E) SCX+ tendons (blue) are shown adjacent to Myosin+ muscle labelled in green. (A-H) The boundaries between muscle and tendons are delineated with dashed lines. (**I-L**) In situ hybridization to adjacent and transverse FCU muscle sections of E10 chicken embryos with the SCX (I), TMEM8C (J), MYOG (K) and MYOD (L) probes, followed by immunohistochemistry with the MF20 antibody (n=3 embryos). (I) Myosins are shown in green adjacent to *SCX* expression in tendons. (I-L) The boundaries between Myosin+ muscle and SCX+ tendons are delineated with dashed lines. In (B-D, J-L) myosin staining (not shown) was used to delineate the boundaries between muscle and tendon, but removed for a clear illustration of the transcript location. *TMEM8C* and *MYOG* transcripts display a central and more restricted expression in muscles compared to those of *MYOD*, which cover the entire muscles.

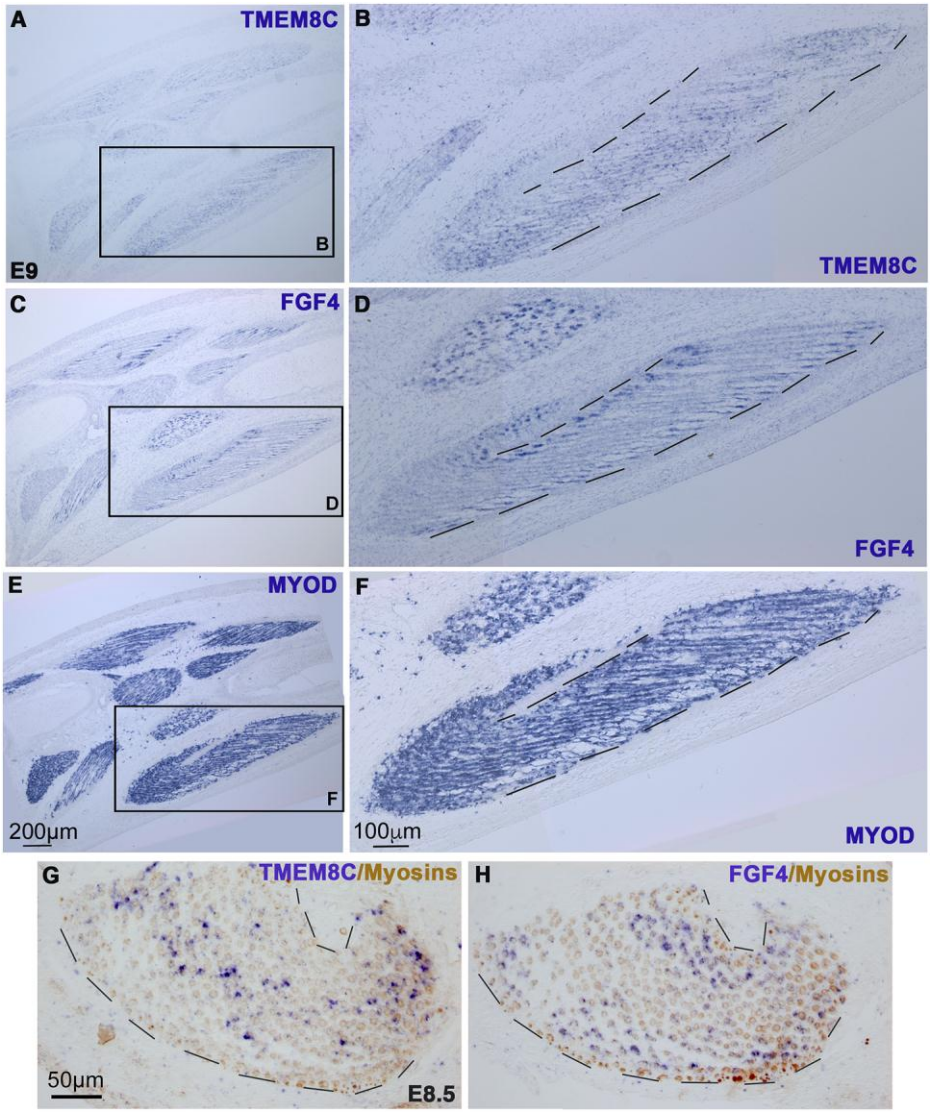

Figure 3. *TMEM8C* transcripts are excluded from muscle tips in limb foetal skeletal muscles

(A-F) In situ hybridization to adjacent and longitudinal limb sections of E8.5 chicken embryos with the TMEM8C (A,B), FGF4 (C,D) and MYOD (E,F) probes (blue). (B,D,F) are high magnifications of FCU muscles in (A,C,E), respectively (n=3 embryos). (**G,H**) In situ hybridization to adjacent and transverse FCU muscle sections of E8.5 chicken embryos with the TMEM8C (G) and FGF4 (H) probes (blue), followed by immunohistochemistry with MF20 antibody to visualise myosins (brown) (n=4 embryos). (A-H) In longitudinal and transverse sections, central *TMEM8C* expression is complementary to that of *FGF4* expression at muscle extremities.

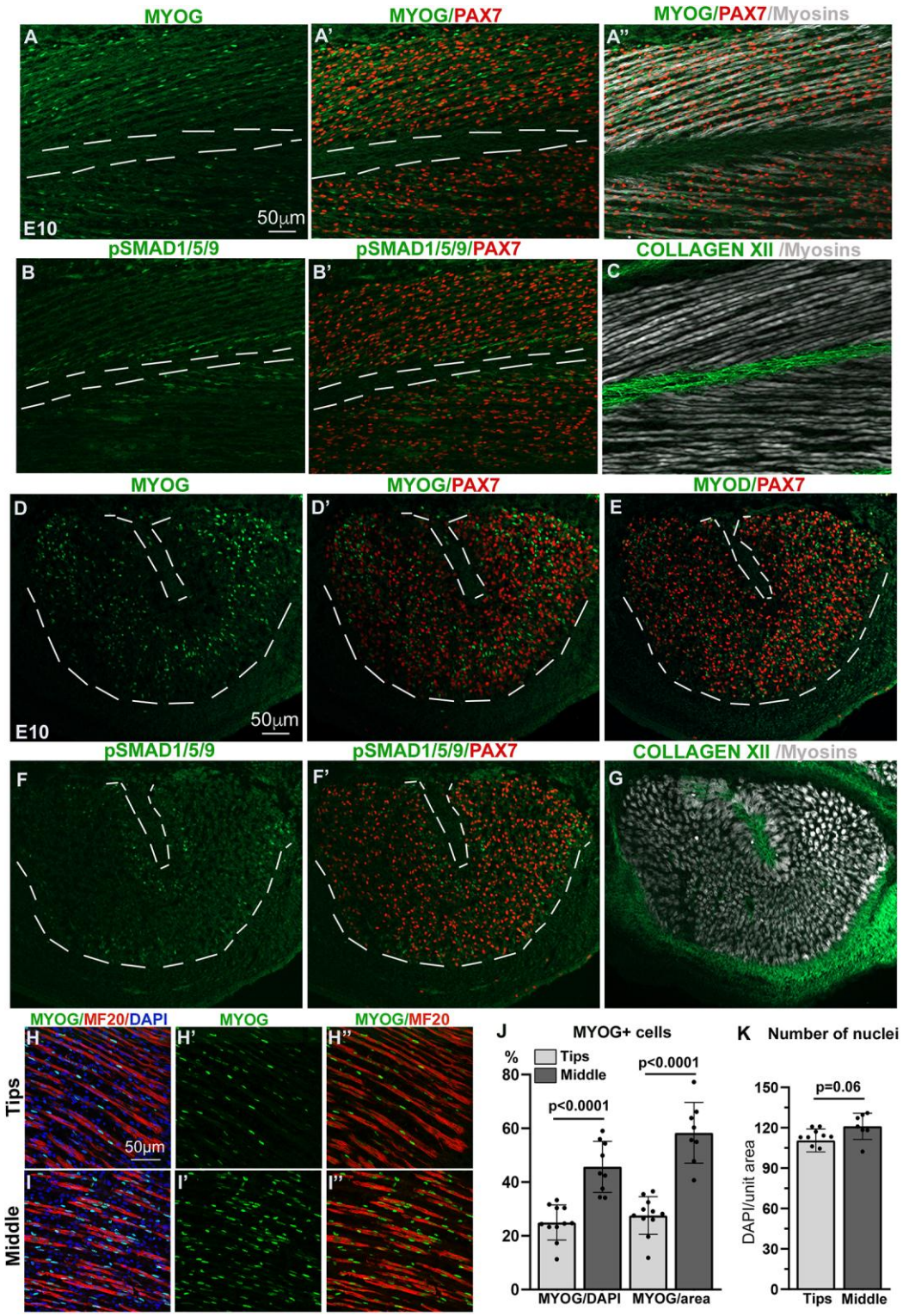

Figure 4. Regionalisation of MYOG+ nuclei in foetal muscles of chicken limbs

(**A-C**) Adjacent and longitudinal limb muscle sections of E10 chicken embryos were co-immunostained with the antibodies MYOG/PAX7/Myosins (A,A',A''), pSMAD1/5/9/PAX7 (B,B') and Collagen XII/Myosins (C) (n=3 embryos). Panels A,A',A'' show the same section labelled with MYOG (A), MYOG/PAX7 (A') or MYOG/PAX7/Myosins (A''). Panels B,B'

show the same section labelled with pSMAD1/5/9 (B) or pSMAD1/5/9/PAX7 (B'). In the panels A,A',B,B', white dashed lines delineate the muscle and tendon interface. (**D-G**) Adjacent and transverse FCU muscle sections of E10 chicken embryos were co-immunostained with the antibodies MYOG/PAX7 (D,D'), MYOD/PAX7 (E), pSMAD1/5/9/PAX7 (F,F') and Collagen XII/Myosins (G) (n=6 embryos). Panels D,D' show the same section labelled with MYOG (D) or MYOG/PAX7 (D'). Panels F,F' show the same section labelled with pSMAD1/5/9 (F) or pSMAD1/5/9/PAX7 (E'). In panels D,D',E,F,F', white dashed lines delineate the muscle and tendon interface. MYOG+ and pSMAD1/5/9+ nuclei are regionalized and display a complementary distribution within muscles. **(H-I'')** Longitudinal limb muscle sections co-immunostained with the antibodies MYOG/Myosins and DAPI to visualise the nuclei (n=3 embryos). Pictures obtained from muscle tips (H,H',H'') and middle of the muscles (I,I',I'') show that MYOG+ cells are not evenly distributed within muscles. **(J)** Percentage of MYOG+ cells and PAX7+ cells at the tips versus the central region of the muscles (n=5 embryos including transverse and longitudinal muscle sections for tips and middle quantification). Graph shows the percentage of cells per total cell number (DAPI+) ± s.d. in each region. **(K)** Percentage of the total nuclei (DAPI+) per area in the tips and in the central region of muscles (n=5 embryos). Graph shows the mean±s.d.

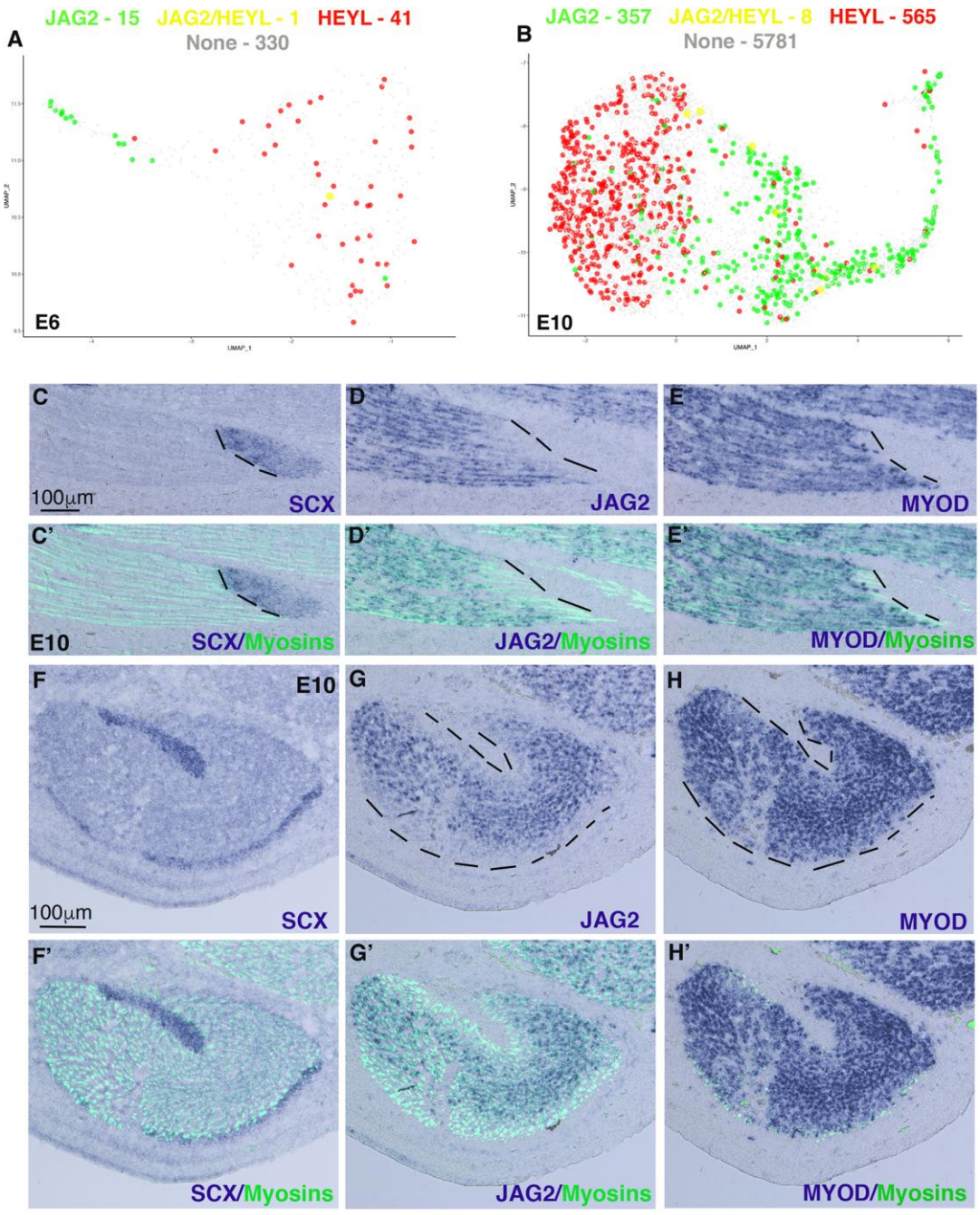

Figure 5. Regionalised expression of the NOTCH ligand JAG2 in foetal muscles of chicken limbs and exclusion of HEYL expression from TMEM8C+ fusion-competent myoblasts

(A,B) Feature plot showing the distribution of *JAG2+* cells (red dots) and *HEYL+* cells (green dots) and double *JAG2+/HEYL+* cells (yellow dots) within muscle clusters at E6 (A) and E10 (B). **(C,H')** In situ hybridization to adjacent longitudinal (C-E') or transverse (F-H') limb sections of E10 chicken embryos with the SCX (C,C',F,F'), JAG2 (D,D',G,G'), and MYOD (E,E',H,H') probes (blue), followed by immunostaining with the MF20 antibody to visualise Myosins (n=4 embryos). Dashed lines delineate the interface between tendon and muscle. *JAG2* expression is reduced in muscle regions close to tendons (D,D',G,G'), while *MYOD* expression covers the entire surface of muscle (E,E',H,H'). **(I)** Bar plot showing the percentage of *HEYL+* cells within the *PAX7+* (red), *MYOD1+* (green), *MYOG+* (blue), *MYH1D+* (purple) populations as well as within the *MYOD1+* and/or *MYOG+*/*TMEM8Cneg* and *TMEM8C+* (blue) populations at E10. Statistical test used is two-sided Fisher's exact test. Sample size: 21256 cells from three E10 embryos. The exact p values are indicated on the graph. Numbers used for percentage calculations in the *PAX7+*, *MYOD1+*, *MYOG+* and *MYH1D+* populations are those of the corresponding co-expression feature plots (data not shown). Numbers used for percentage calculations in the two *MYOD1+* and/or *MYOG+* populations are those of Fig.S6H. **(J)** Visual representation in the form of a Venn diagram showing the distribution of *HEYL+* and *TMEM8C+* cells within the *MYOD1+* and/or *MYOG+* population at E10.

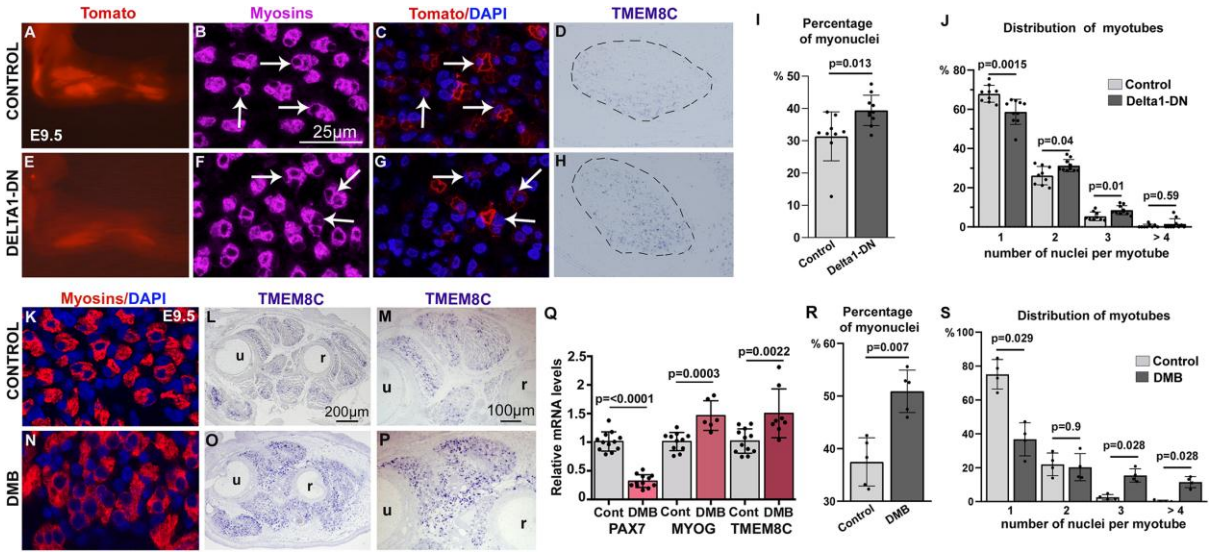

Figure 6. NOTCH loss-of-function increases myoblast fusion and *TMEM8C* expression in limb muscles

(**A-H**) Electroporation of control (Tomato-only, n=3) (A-D) and Tomato-DELTA1-DN (n=3) (E-H) plasmids expressed in differentiated myogenic cells and analysed in E9.5 embryos. (A) Whole-mount electroporated limbs with control plasmid (Tomato, n=3) (A) and with Tomato-DELTA1-DN (n=3) (E). (B,C,F,G) Transverse sections of limb muscles from control (B,C) and DELTA1-DN (F,G) immunostained with MF20 to visualize Myosins (B,F) and Tomato to visualise the electroporated myotubes with the nuclear marker DAPI (C,G). In (B,C,F,G) arrows indicate examples of Tomato+ fibres. (D,H) In situ hybridization to transverse limb sections with the TMEM8C probe of control (D) and DELTA1-DN electroporated embryos (H). **(I)** Percentage of Myosin+ myonuclei among all DAPI+ nuclei in control and DELTA1-DN embryos (n=3 embryos per condition). Graph shows the mean±s.d. **(J)** Distribution of the number of myonuclei per muscle fibre in control and DELTA1-DN embryos (n=3 embryos per condition). Graph shows the mean±s.d. (**K-P**) Limbs of immobilised (DMB treatment) E9.5 embryos were processed for immunohistochemistry (n=3 embryos control and 3 embryos DMB) (K,N) or in situ hybridisation (n=3 embryos control and 3 embryos DMB) (L,M,O,P). (K,N) Transverse sections of limb muscles from control (K) and immobilised (N) embryos were immunostained with MF20 and DAPI to visualise myofibres and nuclei, respectively. (L,M,O,P) Forelimb transverse sections of control (L,M) and immobilised (O,P) embryos were hybridised with TMEM8C probe. (M,P) are high magnifications of dorsal limb muscles of (L,O). (**Q**) RT-qPCR analyses of the mRNA levels for *PAX7* (n=12 control and n=12

DMB), *MYOG* (n=11 control and n=6 DMB),and *TMEM8C* (n=11 control and n=8 DMB),genes in control and immobilised limbs. Graph shows mean±s.d. of gene expression in at least 6 control forelimbs and 6 paralysed forelimbs. The relative mRNA levels were calculated using the $2^{\wedge-\Delta\Delta Ct}$ method. For each gene, the mRNA levels of control limbs were normalised to 1. (**R**) Percentage of Myosin+ myonuclei among all DAPI+ nuclei in control and immobilised embryos (n=3 embryos per condition). (**S**) Distribution of the number of myonuclei per muscle fibre in control and immobilised embryos (n=3 embryos per condition). u, ulna; r, radius.

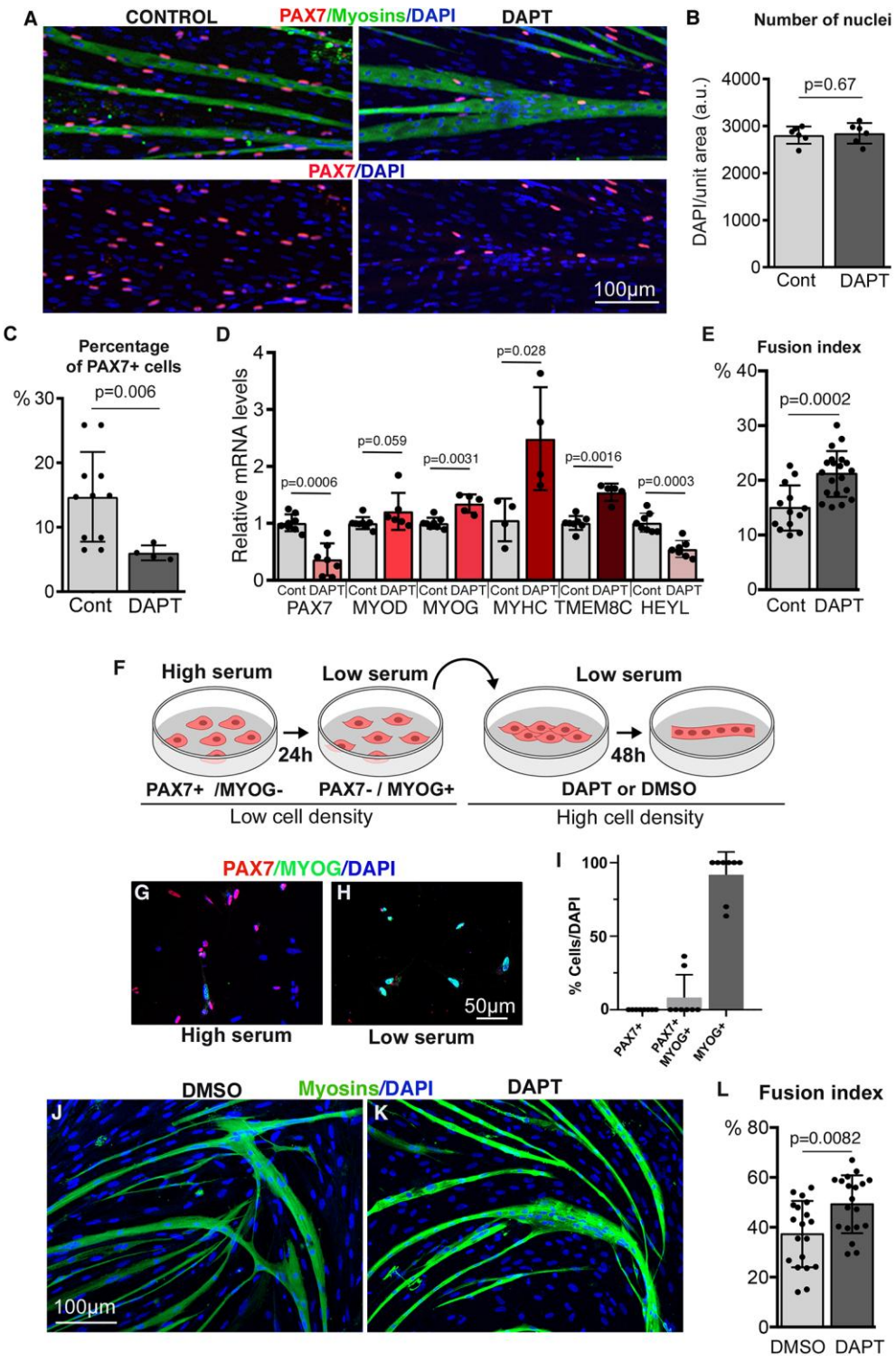

Figure 7. Inhibition of NOTCH activity promotes terminal differentiation and fusion in differentiating foetal myoblast cultures

(**A**) Representative fields of chicken myoblast cultures in differentiation conditions treated with DMSO (control) or DAPT, labelled with PAX7 (muscle progenitors, red) and MF20 (myosins, green) antibodies combined with DAPI staining (nuclei, blue) (n=6 per condition).

(**B**) Density of nuclei in control and DAPT-treated cultures (n=6 per condition). Graph shows mean±s.d., a.u., arbitrary units. (**C**) Percentage of PAX7+ cells with respect to all DAPI+ cells in control and DAPT-treated cultures (n=3 per condition). Graph shows mean±s.d. (**D**) RT-qPCR analyses of the expression levels for muscle markers, *PAX7* (n=8 control, n=7 DAPT), *MYOD* (n=8 control, n=6 DAPT), *MYOG* (n=8 control, n=5 DAPT), *MYHC* (n=4 control, n=4 DAPT), *TMEM8C* (n=8 control, n=5 DAPT) and *HEYL* (n=8 control and n=7 DAPT) in control (grey bars) and DAPT-treated (coloured bars) myoblasts cultured in differentiation conditions. Graph shows mean±s.d. of at least 4 control and 4 DAPT-treated myoblast cultures. (**E**) Fusion index in control (DMSO) and DAPT-treated cultures (n=6 per condition). Graph shows the mean±s.d. (**F**) Scheme of the experimental design to promote myoblast differentiation without fusion. (**G,H**) Myoblasts cultured at low density with proliferation medium (G) and differentiation medium (H), labelled with PAX7 (red) and MYOG (green) antibodies and the nuclear marker DAPI (blue) (n=3 independent experiments). (**I**) Percentage of PAX7+ and MYOG+ cells with respect to all DAPI+ nuclei in myoblast cultures seeded at low cell density and incubated for 24 hours in low serum-containing medium (n=3 independent experiments). (**J,K**) MYOG+ differentiated myoblasts plated at high density were treated with DMSO (J) or DAPT (K) for 48 h and immunostained with MF20 antibody to label myosins (n=3 independent experiments per condition). (**L**) Fusion index in control (DMSO) and DAPT-treated MYOG+ myoblast cultures (n=3 independent experiments per condition). Graph shows the mean±s.d.

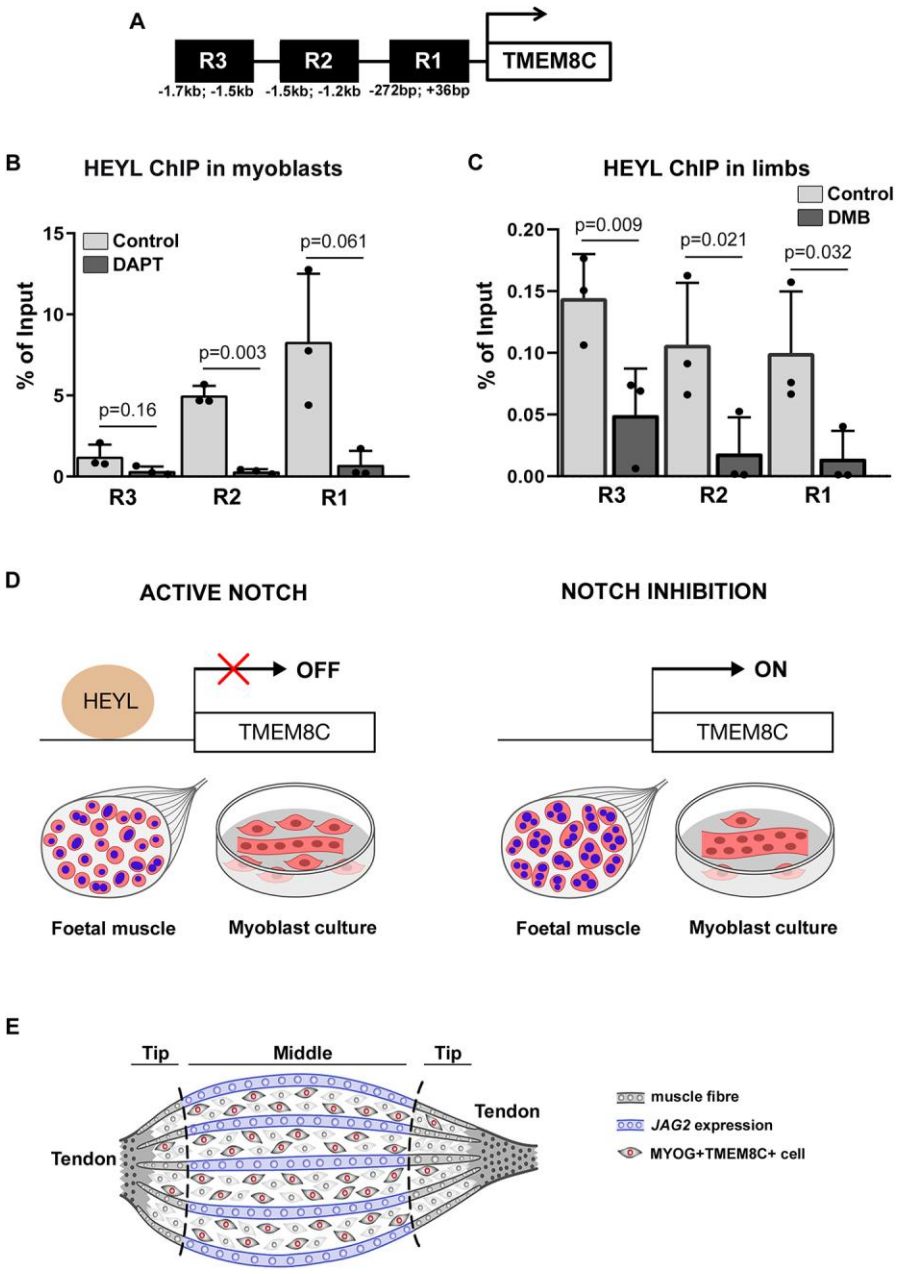

Figure 8. The HEYL repressor is released from *TMEM8C* regulatory regions upon NOTCH inhibition in myoblasts and limb muscles

(**A**) Scheme of the E-box-containing regions upstream the transcription starting site of the *TMEM8C* gene, tested by ChIP-RT-qPCR, R1 (+36 bp; -272 bp), R2 (-1.2 kb; -1.5 kb) and R3 (-1.5 kb; -1.7 kb). (**B,C**) ChIP assays were performed on differentiated myoblast cultures treated with DAPT or DMSO (n=3 independent cultures per condition) (B) and on chicken limb muscles of mobile and immobile embryos (n=3 embryos control and n=3 embryos DMB) (C), with an antibody recognizing HEYL to analyse HEYL recruitment to *TMEM8C*

regulatory regions. Graphs show the mean±s.d. (**D**) Schematic representation of the recruitment of the transcriptional repressor HEYL to the *TMEM8C* regulatory regions in control and NOTCH inhibition conditions in myoblast cultures and foetal limb muscles. **(E)** Schematic representation of the regionalisation of *JAG2* transcripts and MYOG+*TMEM8C*+ fusion-competent cells.

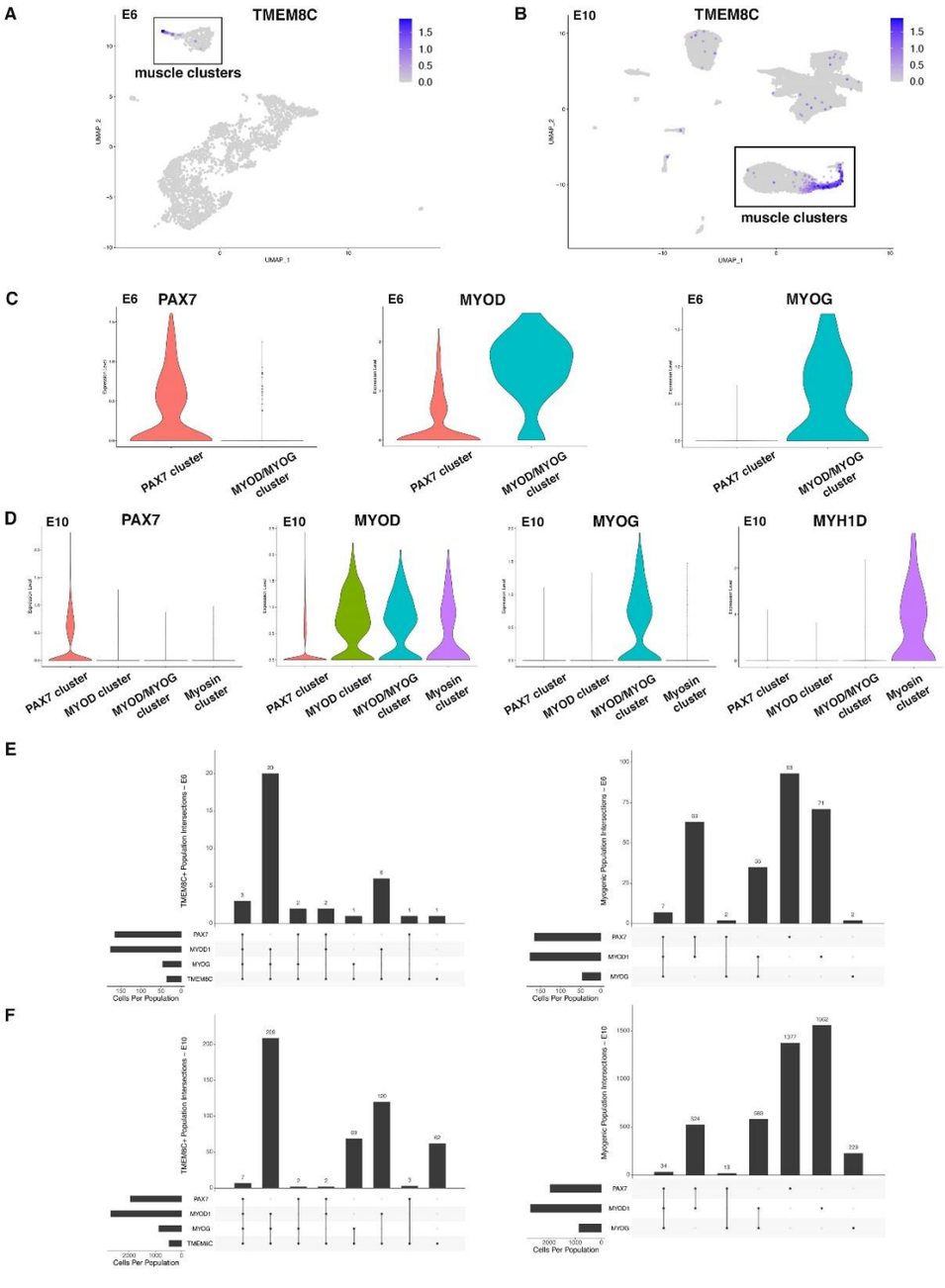

G

	Percentage in TMEM8C+ population	
Major gene combinations	E6	E10
TMEM8C/MYOD/MYOG	55,5	44,1
TMEM8C/MYOD	16,7	25,3
TMEM8C/MYOG	2,8	14,5
3 combinations altogether	75	84

	Percentage in myogenic population	
Corresponding gene combinations	E6	E10
MYOD/MYOG	12,8	13,5
MYOD	26	36,1
MYOG	0,7	5,3
3 combinations altogether	39,6	54,8

Figure S1

Fig. S1. *TMEM8C* is co-expressed with *MYOD* and *MYOG* in limb foetal muscles

(**A,B**) Feature plots showing the distribution of *TMEM8C*+ cells across all limb clusters at E6 (A) and E10 (B). The muscle clusters are boxed. (**C**) Violin plots showing Log-normalized expression levels of the *PAX7, MYOD* and *MYOG* genes in cells grouped by muscle clusters at E6. (**D**) Violin plots showing Log-normalized expression levels of the *PAX7, MYOD, MYOG* and *MYH1D* genes in cells grouped by muscle clusters at E10. (**E,F**) UpSet plots showing cell numbers for the gene combinations present within the *TMEM8C*+ population (left panel) or within the myogenic (*PAX7*+, *MYOD*+ or *MYOG+)* population (right panel) at E6 (E) and E10 (F). The genes considered for the combinations are *PAX7*, *MYOD* and *MYOG*. The size of each population expressing a gene of interest is shown at the bottom left of the plot. (**G**) Left panel: percentage of gene combinations among the *TMEM8C*+ cell population at E6 and E10. Right panel: percentage of gene combinations among the myogenic (*PAX7*+, *MYOD*+ or *MYOG+)* population at E6 and E10. Numbers used for percentage calculations are those of panels E and F.

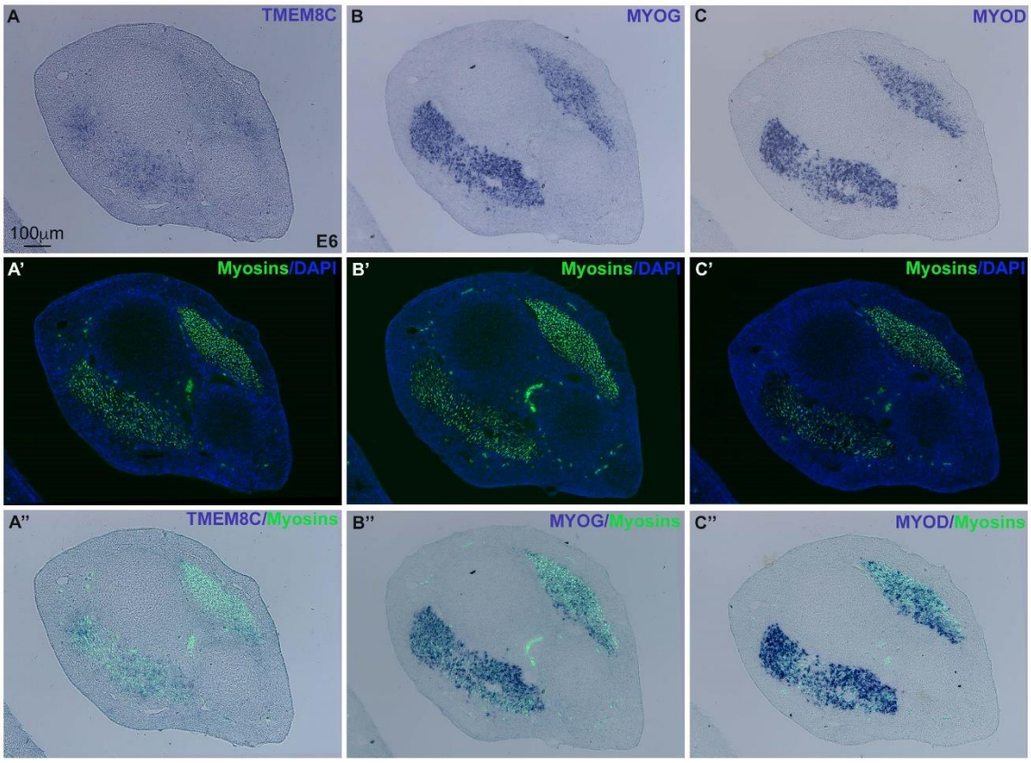

Figure S2

Fig. S2. *MYOD, MYOG* and *TMEM8C* transcripts show a uniform distribution in limb muscle masses of E6 chicken embryos

In situ hybridization to adjacent limb sections of E6 chicken embryos with the TMEM8C (A,A',A''), MYOG (B,B',B'') and MYOD (C,C',C'') probes (blue), followed by immunohistochemistry with the MF20 antibody to visualize myosins (green) and the nuclear marker DAPI (n=4 embryos). (A-C) show in situ hybridization, (A'-C') show myosin expression, (A''-C") show combined in situ hybridization and myosin expression.

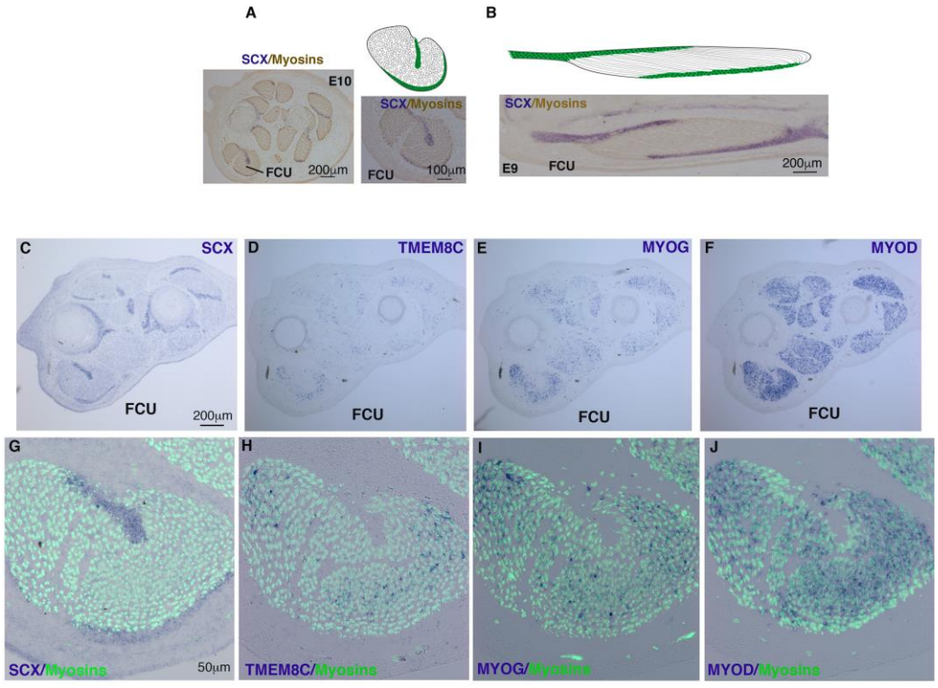

Figure S3

Fig. S3. *TMEM8C* and *MYOG* transcripts are regionalized in foetal muscles of E10 chicken limbs

(**A,B**) Schematic representation of FCU muscle and adjacent tendons. Transverse (A) and longitudinal (B) views to visualise the muscle and tendon interface. (A,B) Tendon are in green in the schematics; In situ hybridization to transverse (A) and longitudinal (B) sections of the FCU muscle with SCX probe (blue) followed by immunohistochemistry with the MF20 antibody to visualize myosins (brown). (**C-J**) In situ hybridization to adjacent and transverse limb sections of E10 chicken embryos with the SCX (C,G), TMEM8C (D,H), MYOG (E,I) and MYOD (F,J) probes (blue), followed by immunohistochemistry with the MF20 antibody to visualize myosins (green) (n=5 embryos). (G-J) are high magnification of the FCU muscle shown in (C,F). *TMEM8C* and *MYOG* transcripts display a regionalized expression in muscles with less intense expression close to SCX+ tendons.

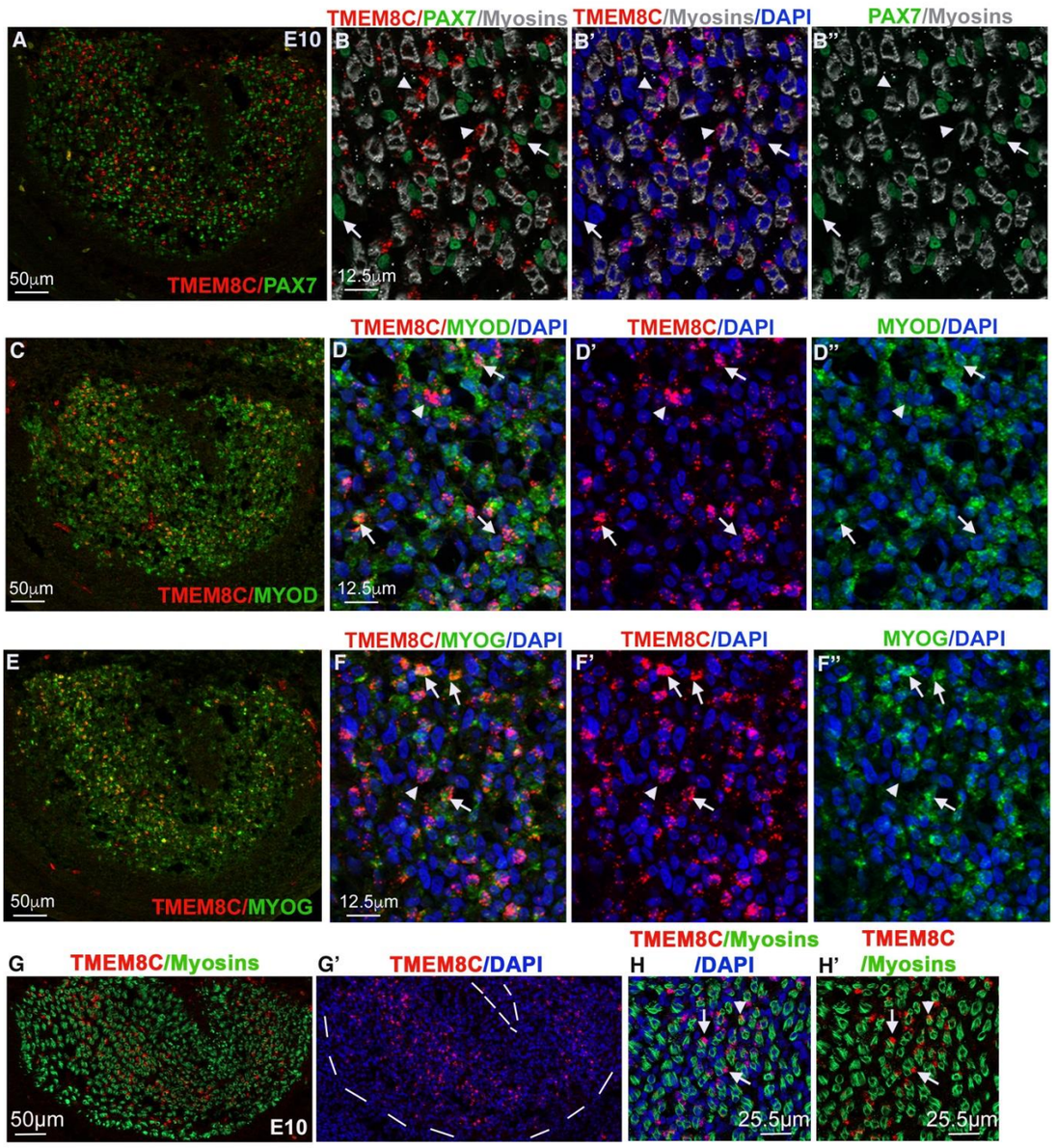

Figure S4

Fig. S4. *TMEM8C* is preferentially expressed in *MYOG*+ cells outside myosin+ myotubes and excluded from PAX7+ progenitors.

(A,B,B',B'') Fluorescent RNA in situ hybridization to transverse limb muscle sections of E10 chicken embryos with the *TMEM8C* probe (red), followed by immunohistochemistry with the PAX7 antibody (green) and MF20 antibody to visualize myosins (grey). (B,B',B'') are high magnification of the FCU muscle shown in (A). Arrowheads point to *TMEM8C* expressing cells (red), while arrows point to PAX7+ cells (green). **(C,D,D',D'')** Double in situ hybridisation to transverse limb muscle section at E10 with *TMEM8C* (red) and *MYOD* (green) probes. (D,D',D'') are high magnification of the FCU muscle shown in (C). Arrows point to *TMEM8C+MYOD+* cells (red and green), while arrowheads point to *TMEM8C+MYOD-* cells (red). **(E,F,F',F'')** Double in situ hybridisation to transverse limb muscle section at E10 with *TMEM8C* (red) and *MYOG* (green) probes. (F,F',F'') are high magnification of the FCU muscle shown in (E). Arrows point to *TMEM8C+MYOG+* cells (red and green), while arrowheads point to *TMEM8C+* cells (red) that are not *MYOG+* cells. (**G,G',H,H'**) Fluorescent in situ hybridization to transverse limb muscle sections of E10 chicken embryos with the *TMEM8C* probe (red), followed by immunohistochemistry with the MF20 antibody to visualize myosins (green). (H,H') is a higher magnification of (G). *TMEM8C* transcripts (red, arrows) are preferentially observed outside myotubes (green), although we could detect rare myotube expressing *TMEM8C*, n=5 embryos.

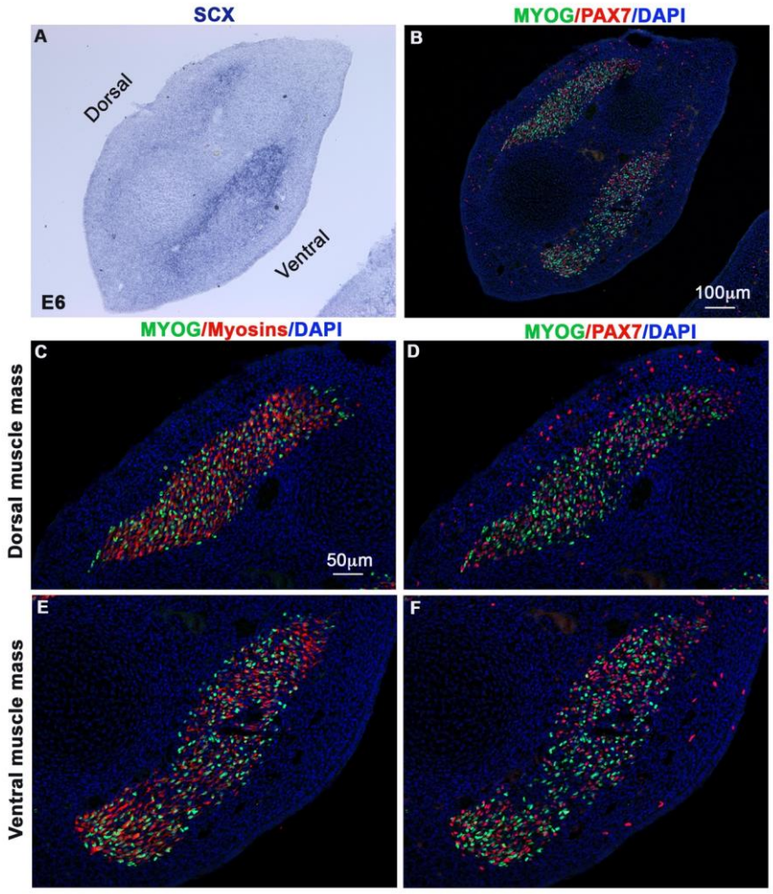

Figure S5

Fig. S5. MYOG + cells are not regionalized in limb muscle masses of E6 chicken embryos

(**A,B**) Adjacent limb transverse sections of E6 chicken embryos were hybridized with the SCX probe (A) and co-immunostained with MYOG (green) and PAX7 (red) antibodies, and DAPI to visualise nuclei (n=3 embryos). **(C-F)** Adjacent limb transverse sections of E6 chicken embryos were co-immunostained with MYOG (green) and MF20 (red), to visualise myosins, (C,E) and MYOG (green) and PAX7 (red) (D,F), with DAPI to visualise nuclei (C-F). (D, F) are high-magnifications of B. (C,D) and (D,F) show dorsal and ventral muscle masses, respectively.

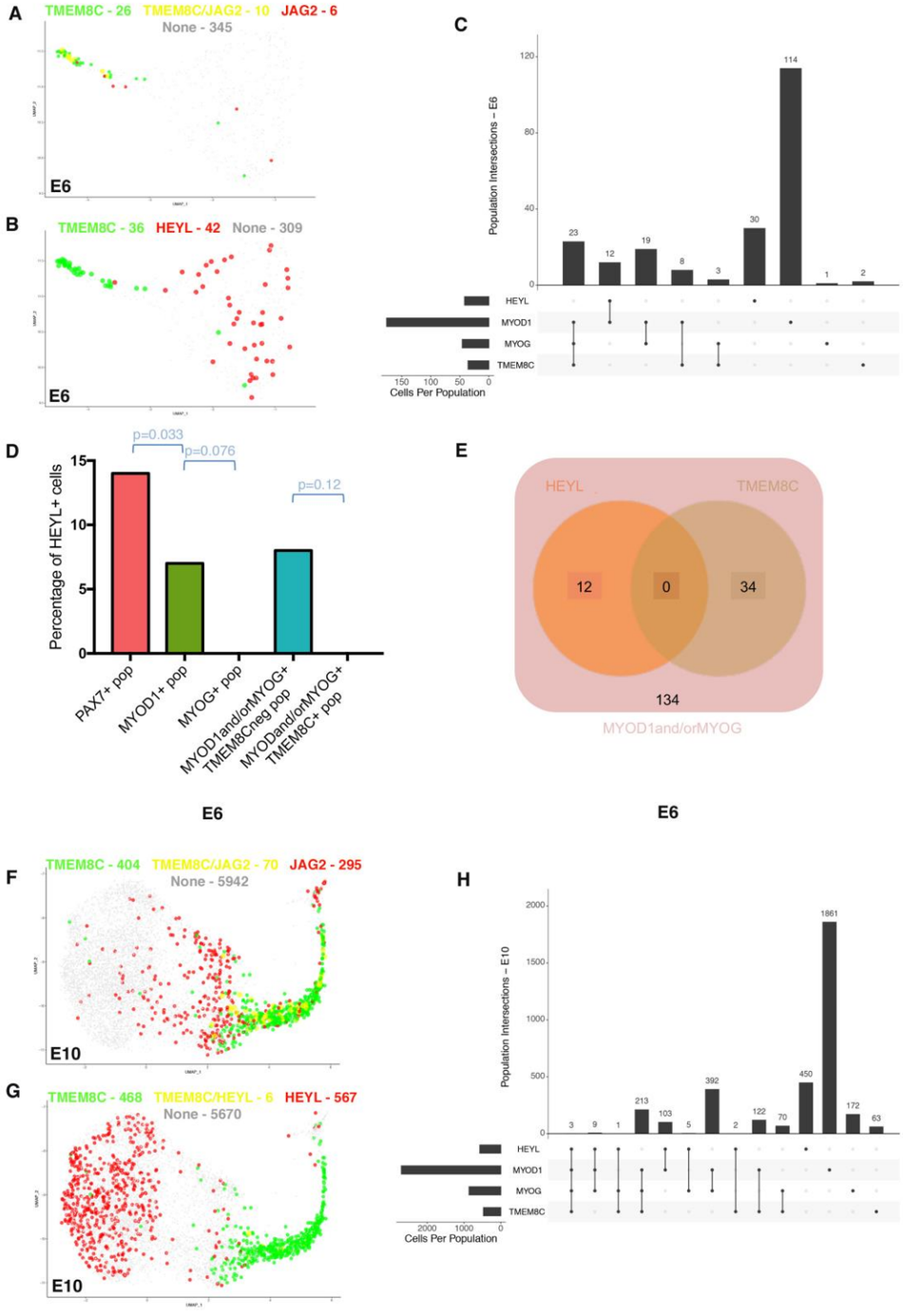

Figure S6

Fig. S6. Unlike *JAG2*, *HEYL* expression does not overlap with *TMEM8C* expression at E6 and E10.

(**A,F**) Feature plot showing the distribution of *TMEM8C*+ cells (green dots) and *JAG2*+ cells (red dots) and double *TMEM8C*+/*JAG2*+ cells (yellow dots) within muscle clusters at E6 (A) and E10 (F). (**B,G**) Feature plot showing the distribution of *TMEM8C*+ cells (green dots) and *HEYL*+ cells (red dots) and double *TMEM8C*+/*HEYL*+ cells (yellow dots) within muscle clusters at E6 (B) and E10 (G). (**C,H**) UpSet plots showing cell numbers for the gene combinations present within the *MYOD1*+ and/or *MYOG*+ population at E6 (C) and E10 (H). The genes considered for the combinations are *HEYL*, *MYOD1*, *MYOG* and *TMEM8C*. The size of each population expressing a gene of interest is shown at the bottom left of the plot. **(D)** Bar plot showing the percentage of *HEYL*+ cells within the *PAX7*+ (red), *MYOD1*+ (green), *MYOG*+ (blue) populations as well as within the *MYOD1*+ and/or *MYOG*+/*TMEM8Cneg* and *TMEM8C*+ (blue) populations at E6. Statistical test used is two-sided Fisher's exact test. Sample size: 3268 cells from three E6 embryos. The exact p values are indicated on the graph. Numbers used for percentage calculations in the *PAX7*+, *MYOD1*+ and *MYOG*+ populations are those of the corresponding co-expression feature plots (data not shown). Numbers used for percentage calculations in the two *MYOD1*+ and/or *MYOG*+ populations are those of panel C. **(E)** Visual representation in the form of a Venn diagram showing the distribution of *HEYL*+ and *TMEM8C*+ cells within the *MYOD1*+ and/or *MYOG*+ population at E6.

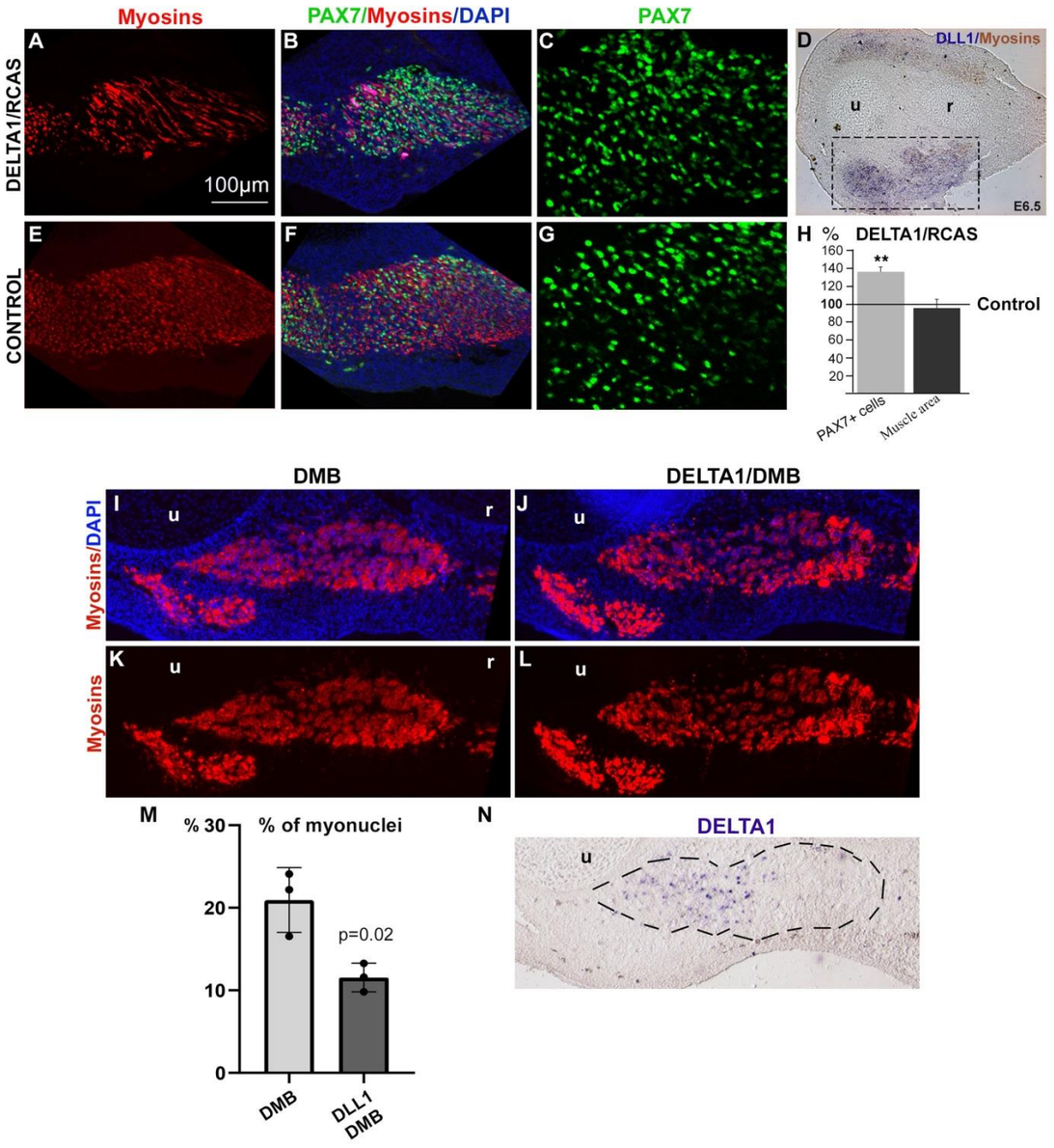

Figure S7

Fig. S7. DELTA1 activated NOTCH prevents the increase of myoblast fusion observed in DMB limbs

(**A-G**) DELTA1/RCAS-expressing cells were grafted into the presumptive right forelimb buds of E4.5 chicken embryos, the contralateral limb of the same embryo was used as control (n=3 embryos). DELTA1-grafted right (A-D) and control left (E-G) forelimbs from E6.5

chicken embryos were cut transversely and analysed for *DLL1* transcripts (D) and immunostained with the PAX7 (green) and MF20 (myosins, red) antibodies (A-C,E-G). (**H**) Percentage of PAX7+ cells with respect to the muscle area and percentage of the muscle area (MF20 area), in muscle regions of DELTA1-grafted and control forelimbs from E6.5 chicken embryos (n=3 embryos). (**I-L**) Limb transverse sections of E9.5 DMB-treated embryos (I,J) and DELTA1-grafted embryos treated with DMB (K,L) immunostained with MF20 to visualise myosins (red) and DAPI (blue) to visualise the nuclei. (**M**) Quantification of the number of myonuclei in MF20+ myotubes versus total DAPI. Graph shows the percentage of cells per area ± s.d. (n=3 embryos). (**N**) In situ hybridization for *DLL1* (blue) shows ectopic expression of *DLL1* in DELTA1-grafted embryos treated with DMB. (N) is an adjacent section to (J,L) of the same embryo.

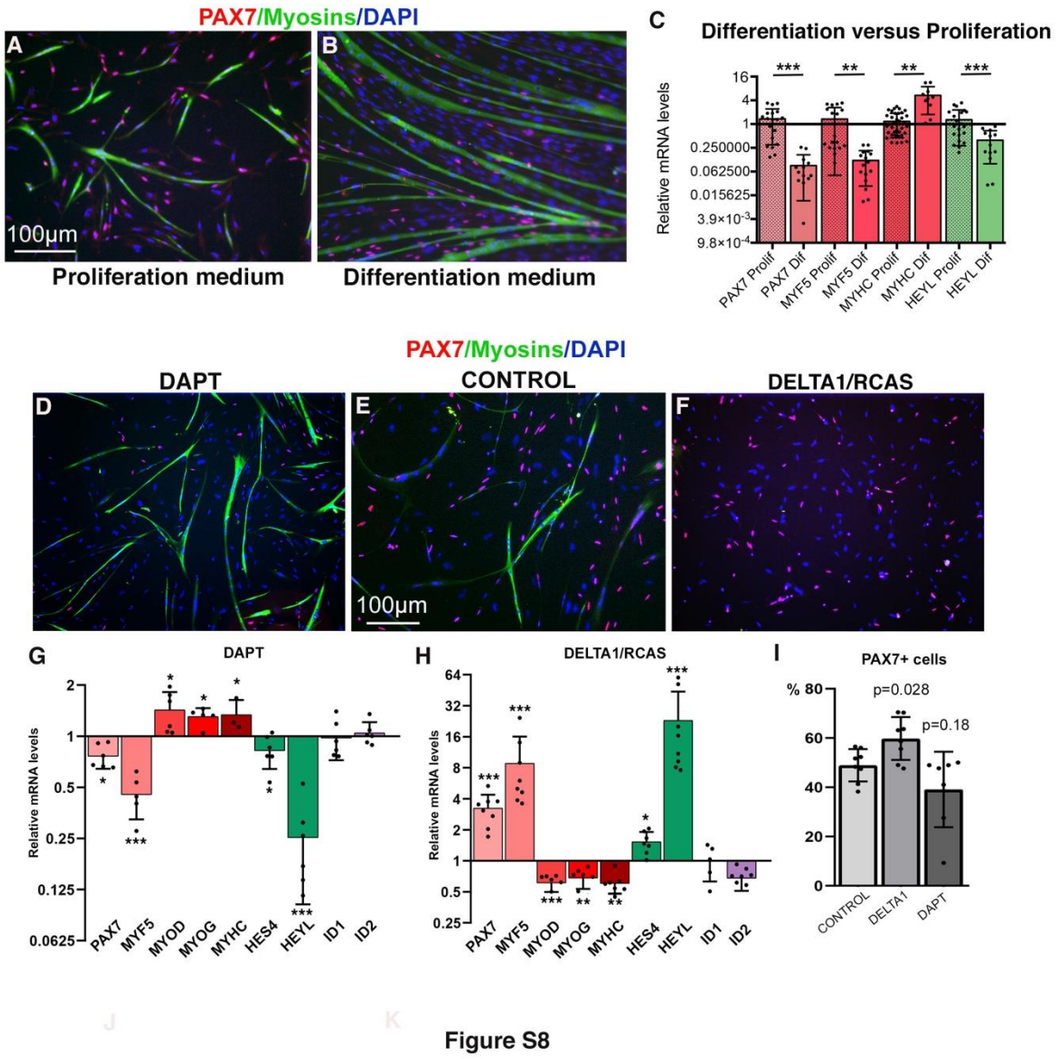

Figure S8

Fig. S8. A myoblast culture system that mimics in vivo myogenesis

(**A,B**) Representative fields of proliferating (A) and differentiating (B) chicken myoblasts labelled with PAX7 (red) and MF20 (green), to visualise myosins, and with the nuclear marker DAPI (n=12 independent cultures). (**C**) RT-qPCR analyses of the mRNA expression levels for the muscle markers, *PAX7*, *MYF5*, *MYHC* and the NOTCH target gene *HEYL*, in differentiation (*PAX7* n=12, *MYF5* n=15, *MYHC* n=9, *HEYL* n=12) versus proliferation (*PAX7* n=18, *MYF5* n=17, *MYHC* n=35, *HEYL* n=20) culture conditions. The mRNA levels

of the genes of myoblasts in proliferation conditions were normalised to 1 (control) and the relative mRNA levels of the genes in differentiation conditions was calculated versus the expression in proliferating conditions. Graph shows mean±s.d. (**D-F**) Representative fields showing PAX7+ (red) and myosin+ (green) cells in chicken foetal myoblasts treated with DAPT (D), transfected with Empty/RCAS (E) or transfected with DELTA1/RCAS (F), and cultured in proliferation conditions (n=5 independent cultures). (**G,H**) RT-qPCR analyses of the expression levels for muscle markers, NOTCH target genes and BMP target genes in DAPT-treated (G) (*PAX7* n=6, *MYF5* n=5, *MYOD* n=6, *MYOG* n=5, *MYHC* n=3, *HES4* n=6, *HEYL* n=6, *ID1* n=6, *ID2* n=6) and DELTA1/RCAS-infected (H) (*PAX7* n=8, *MYF5* n=8, *MYOD* n=6, *MYOG* n=6, *MYHC* n=7, *HES4* n=7, *HEYL* n=8, *ID1* n=5, *ID2* n=7) myoblasts cultured in proliferation conditions. The relative mRNA levels were calculated using the $2^{-\Delta\Delta Ct}$ method. For each gene, the mRNA levels of Empty/RCAS-infected myoblasts (control) were normalised to 1. Graph shows mean±s.d. *p<0.05; ** p<0.01; *** p<0.001. (**I**) Percentage of PAX7+ cells with respect to all DAPI+ cells in control, DAPT-treated and DELTA1 cultures (control n=8, DELTA1 n=8, DAPT n=7).

.

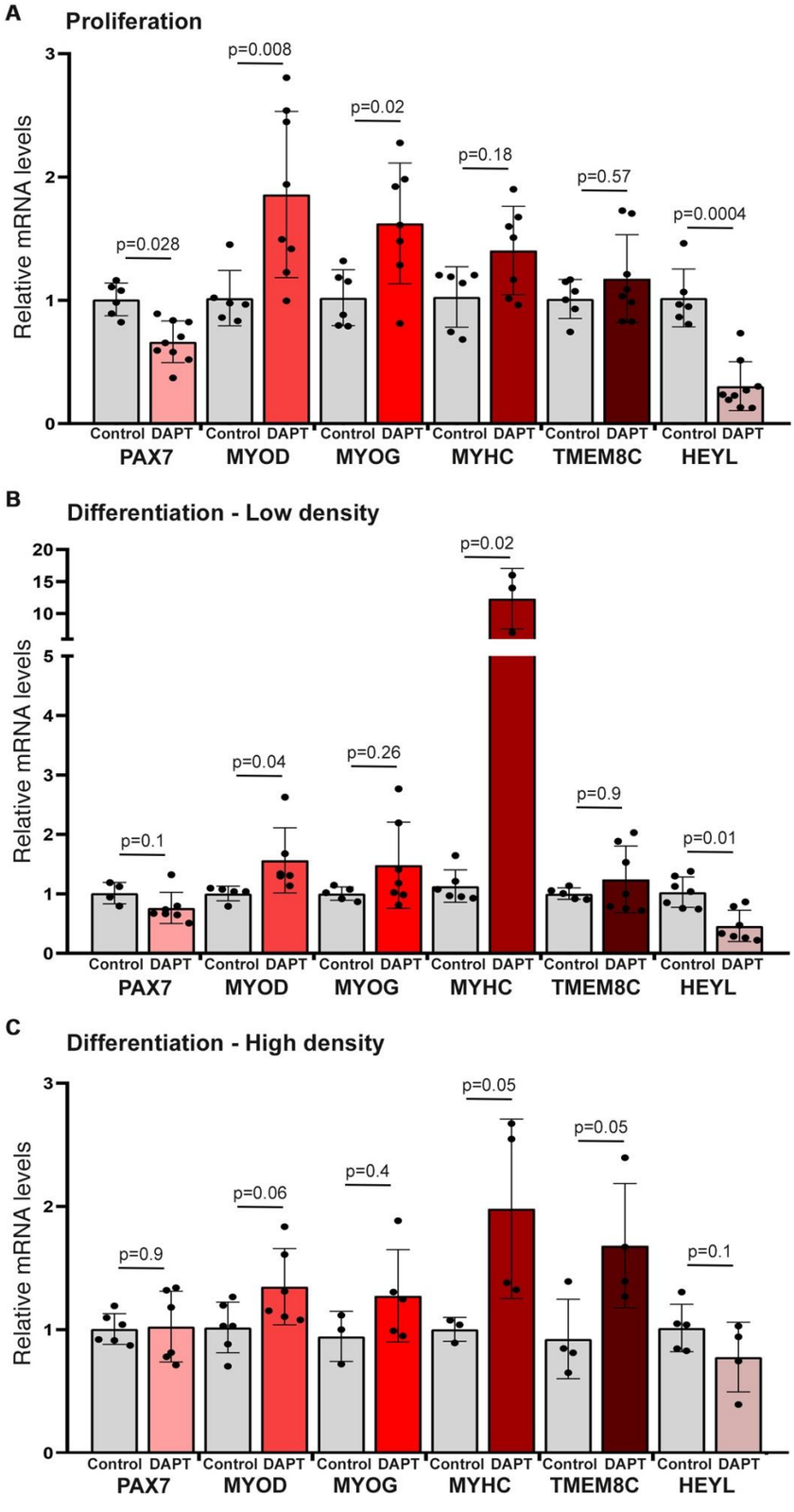

Figure S9

Fig. S9. Inhibition of NOTCH increases *TMEM8C* expression in the differentiation and high confluence condition in the 2-step culture system.

(**A**) Myoblasts cultured at low density with proliferation medium. RT-qPCR analyses of the expression levels for muscle markers and *HEYL* (NOTCH target gene) in control myoblasts (*PAX7* n=6, *MYOD* n=6, *MYOG* n=6, *MYHC* n=6, *TMEM8C* n=6, *HEYL* n=6) and DAPT-treated myoblasts (*PAX7* n=9, *MYOD* n=8, *MYOG* n=7, *MYHC* n=7, *TMEM8C* n=8, *HEYL* n=9) cultured at low density and in proliferation conditions. (**B**) Myoblasts cultured at low density with differentiation medium. RT-qPCR analyses of the expression levels for muscle markers and *HEYL* (NOTCH target gene) in control myoblasts (*PAX7* n=4, *MYOD* n=5, *MYOG* n=5, *MYHC* n=6, *TMEM8C* n=5, *HEYL* n=7) and DAPT-treated myoblasts (*PAX7* n=7, *MYOD* n=6, *MYOG* n=6, *MYHC* n=3, *TMEM8C* n=7, *HEYL* n=7) cultured at low density and in differentiation conditions. (**C**) Myoblasts cultured at high density with differentiation medium. RT-qPCR analyses of the expression levels for muscle markers and *HEYL* (NOTCH target gene) in control myoblasts (*PAX7* n=6, *MYOD* n=6, *MYOG* n=3, *MYHC* n=3, *TMEM8C* n=4, *HEYL* n=5) and DAPT-treated myoblasts (*PAX7* n=6, *MYOD* n=6, *MYOG* n=5, *MYHC* n=4, *TMEM8C* n=4, *HEYL* n=4) cultured at high density and in differentiation conditions. The relative mRNA levels were calculated using the $2^{\wedge-\Delta\Delta Ct}$ method. For each gene, the mRNA levels of control myoblasts were normalised to 1. Graph shows mean±s.d. p values are indicated on the graphs.

Table S1. List of antibodies.

Antibody	Validation	Source	Reference	Dilution
Mouse monoclonal IgG2b anti-MYHC	https://dshb.biology.uiowa.edu/MF-20	DSHB	MF20	IF supernatant
Mouse monoclonal IgG1 anti-PAX7	https://dshb.biology.uiowa.edu/PAX7	DSHB	PAX7, lot 20ea1/24/19	IF (1:200)
Mouse polyclonal anti-MYOD	Manceau et al., 2008	produced in the lab	554130, lot 9011506	IF (1:100)
Rabbit polyclonal anti-MYOG	Manceau et al., 2008	produced in the lab	lot HL1510	IF supernatant
Rabbit polyclonal anti-Collagen type XII	Koch et al, 1992	produced in the lab	Clone 522	IF (1:100)
Rabbit polyclonal anti-pSMAD1/5/9	https://www.cellsignal.com/products/primary-antibodies/phospho-smad1-5-ser463-465-41d10-rabbit-mab/9516	Cell Signalling	9516, lot 9	IF (1:100)
Rabbit polyclonal anti-HEYL	Fukada et al., 2007	produced in the lab	NM_013905	ChIP (5µg/IP)

Table S2. List of primers.

RT-qPCR	Forward	Reverse
PAX7	5'-AGAAGAAGGCCAAGCACAGCATAG-3'	5'- ATTCGACATCGGAGCCTTCATCCA-3'
MYF5	5'-ACCAGAGACTCCCCAAAGTG-3'	5'-TCGATGTACCTGATGGCGTT-3'
MYOD	5'-CGACAGCAGCTACTACACGGAAT-3'	5'-CTCTTCCCATGCTTTGGGTC-3'
MYOG	5'-AGGCTGAAGAAGGTGAACGAAG-3'	5'-CAGAGTGCTGCGTTTCAGAGC-3'
MYHC	5'-TGACAACTCCTCACGCTTTG-3'	5'- CTCTGGCTTCTTGTTGGA-3'
TMEM8C	5'-TGGGTGTCCCTGATGGC-3'	5'-CCCGATGGGTCCTGAGTAG-3'
HEYL	5'-CCAAGCTGGAGAAGGCAGA-3'	5'-CCAGAGCACGAGCATCCA-3'
HES4	5'-GCCGGACAAACCTCGGA-3'	5'-CATCCGCTGCCATTTACCTT-3'
ID1	5'-CCGGAGGGTCTCTAAAGTGG-3'	5'-GCAGGTCCCAGATGTAGTCG-3'
ID2	5'-GAAGAACGGCCTTTCGGAG-3'	5'-TCATGTTGTACAGCAGGCTCA-3'
ChIP RT-qPCR	**Forward**	**Reverse**
R1	5'-GTGCATCACAGCCAGCATG-3'	5'-GGTGGGCAGGAGGAGTTT-3'
R2	5'-CACAGTTGCACGTCCATGC-3'	5'-CAACCTGAATGATTCTGTGGTTCTG-3'
R3	5'-GCTGCAAATCAAGCACCGG-3'	5'-CAAACCGTTGTCACACAACCC-3'